

A Combined Experimental and Theoretical Study of Conformational Preferences of Molecular Semiconductors

Jessica E. Coughlin,^{†,‡} Andriy Zhugayevych,[‡] Ronald C. Bakus, II,[†] Thomas S. van der Poll,^{†,‡} Gregory C. Welch,^{†,||} Simon J. Teat,[§] Guillermo C. Bazan,^{*,†} and Sergei Tretiak^{*,‡}

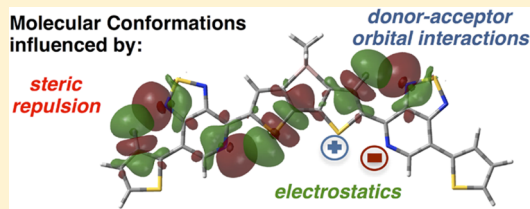
[†]Center for Polymers and Organic Solids, Departments of Chemistry & Biochemistry and Materials, University of California, Santa Barbara, California 93106, United States

[‡]Center for Integrated Nanotechnologies, Los Alamos National Laboratory, Los Alamos, New Mexico 87545, United States

[§]Advanced Light Source, Lawrence Berkeley National Laboratory, Berkeley, California 94720, United States

S Supporting Information

ABSTRACT: Structural modules used for assembling molecular semiconductors have typically been chosen to give desirable optical and electronic properties. Growing evidence shows that chemical functionalities should be considered for controlling molecular shape, which is important for function because of its influence on polymer secondary structure, lattice arrangements in crystals, and crystallization tendencies. Using density functional theory (DFT) calculations, followed by a natural bond orbital (NBO) analysis, we examine eight molecular semiconductors with resolved single crystal X-ray structures to understand the features that dominate molecular conformations and ultimately develop practical rules that govern these preferences. All molecules can be described by a D'-A-D-A-D' architecture and have a 4,4-dimethyl-4H-silolo[3,2-*b*:4,5-*b'*]dithiophene (DTS) donor (D) core unit, with [1,2,5]thiadiazolo[3,4-*c*]pyridine (PT), 5-fluorobenzo[*c*][1,2,5]thiadiazole (FBT), or benzo[1,2,5]thiadiazole (BT) electron acceptor (A) units, and either thiophene, 5-hexyl-2,2'-bithiophene, or benzofuran electron-donating end-caps (D'). The NBO analysis shows that the energy difference between the two alternative conformations, or rotamers, (ΔE_{rot}) is a delicate balance of multiple competing nonbonding interactions that are distributed among many atoms. These interactions include attractive "donor–acceptor" electron sharing, steric repulsion, and electrostatic stabilization or destabilization. A proper grouping of these interactions reveals two primary factors determining ΔE_{rot} . The first concerns heteroatoms adjacent to the bonds connecting the structural units, wherein the asymmetric distribution of π -electron density across the link joining the units results in stabilization of one of two rotamers. The second factor arises from electrostatic interactions between close-contact atoms, which may also shift the ΔE_{rot} of the two rotamers. When all these constituent interactions cooperate, the dihedral angle is "locked" in a planar conformation with a negligible population of alternative rotamers.



INTRODUCTION

Organic semiconductors have become an important topic of research due to their potential incorporation in electronic applications, such as organic photovoltaics and light-emitting diodes.^{1–3} Within the scope of organic photovoltaics (OPVs), the design and synthesis of electron donor materials for use in bulk heterojunction cells has been of particular interest.^{4–8} Although polymeric systems have traditionally shown higher power conversion efficiencies, small molecules have recently proven to be competitive.^{9–13} These molecular semiconductors have the advantage over polymers in that they are monodisperse and amenable to a larger array of purification and characterization techniques, such as single-crystal X-ray diffraction.^{5,14} These structural insights have proven to be useful when evaluating the morphological organizations of these materials in the solid state, which control relevant properties such as exciton migration and charge transport.^{14–20}

Design rules are available for creating high-performance donor materials for OPV applications.^{21–24} One strategy that

has been proven to create high-efficiency materials is the push–pull chromophore design.^{2,25} This architecture of polymeric and molecular semiconductors is created by the alternation of an electron rich (donor, D) unit and an electron deficient (acceptor, A) unit. By careful selection of donor and acceptor units based on electronic character, one can tailor molecular orbital energy levels in order to obtain useful optical band gaps and molecular orbital alignments with other relevant device components.²⁶ Computational methods, such as density functional theory (DFT), have been helpful in the design and understanding of how different chromophore units come together to define optical transitions and orbital energy levels.^{27–29}

Molecular conformations have been shown to influence crystal packing and overall intermolecular self-assembly.^{5,16,30} An important feature to consider is the planarity of the backbone

Received: June 26, 2014

Published: June 27, 2014



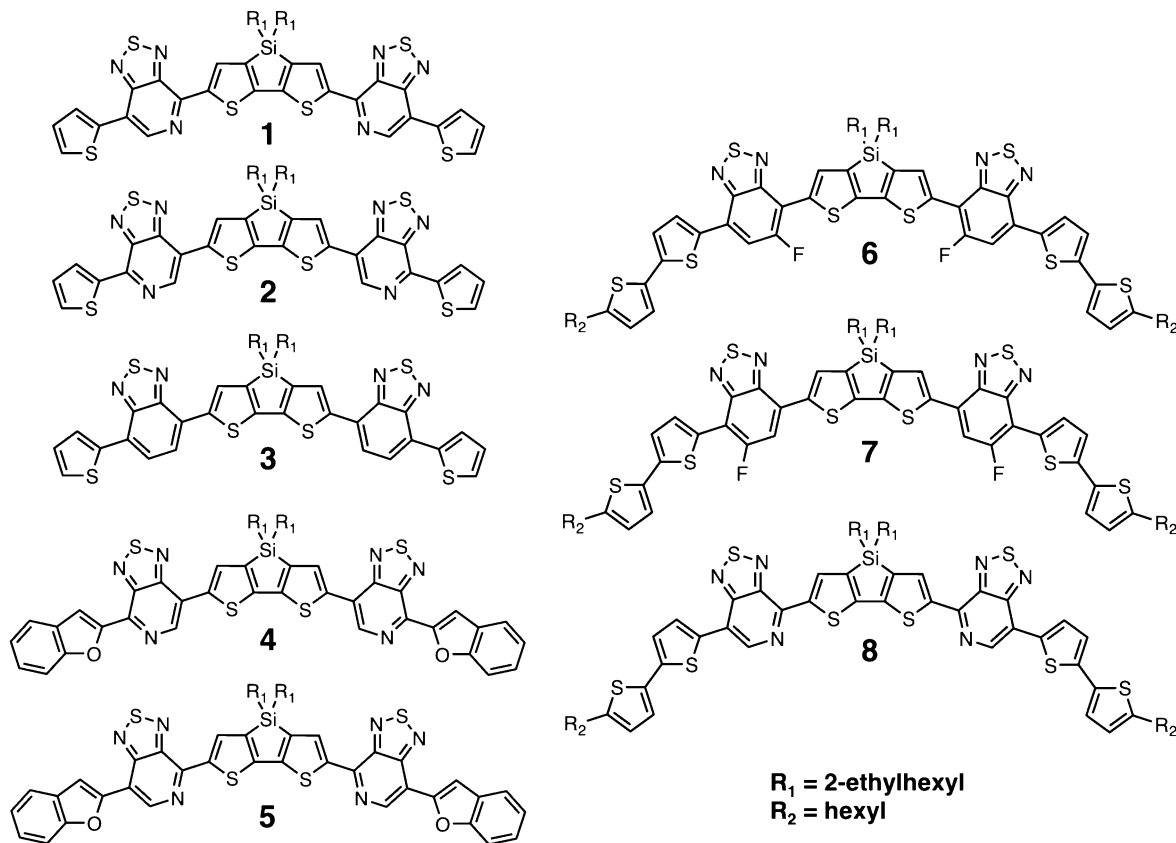


Figure 1. Structures of molecules 1–8.

due to the fact that “kinking” is believed to impede cofacial interactions, thereby decreasing the proximity of the π -delocalized frameworks.^{31,32} A characteristic of the push–pull architecture that has been traditionally overlooked is that the structural components typically contain heteroatoms, which influence the preferred molecular conformation through intramolecular interactions. Conformational “locks” have thus gained attention because of their ability to induce planar molecular structures.³³ Observations show that in close proximity, S and O,^{34–36} S and N,^{30,37,38} and N and H^{5,38} can restrict rotation about bonds linking aromatic units and bring dihedral angles closer to zero. The evidence for these interactions has mostly been explained through van der Waals radii, determined from atomic distances in crystals. Recent systematic first-principles investigations^{39,40} show the same trend and estimate the strength of these interactions to be on the order of 1–2 kcal/mol. Some of these studies have the disadvantages of being done for polymer systems, which do not have the structural precision available for molecular systems.

The considerations mentioned above have important consequences for performance of small molecule semiconductors in organic photovoltaics. For example, Figure 1 displays the members of a class of small molecules with a general D’–A–D–A–D’ architecture, some of which have been recently reported to achieve excellent solar cell power conversion efficiencies.^{10,13,30,41,42} It has also been shown that the choice of heteroatoms can be modulated to change optical transitions, device parameters, and facilitate different device architectures.^{10,43} Despite these empirical successes, a complete picture of how molecular connectivity leads to structural stability, solid-state organization, and ultimately to device performance remains lacking.

In this contribution, we take advantage of a range of crystallographically resolved chromophores of relevance to semiconductor design (Figure 1) and combine this information with ab initio calculations to specifically address the challenge of controlling molecular shape within a solid-state organization. This correlation of theoretically and experimentally determined structural insight has not been previously achieved in calculations for polymer systems. The latter can be ultimately used to estimate electronic properties. In this work, we lay the groundwork for how these types of calculations can be used to predict molecular shape and identify the types of through-space interactions that are important for controlling conformation. An additional novel feature of this work is the use of natural bonding orbital (NBO) analysis to examine the contribution of different interactions that lead to geometric preferences.

All molecules have a 4,4-dimethyl-4H-silolo[3,2-b:4,5-b']dithiophene (DTS) donor (D) core unit, with [1,2,5]thiadiazolo[3,4-c]pyridine (PT), 5-fluorobenzof[*c*][1,2,5]thiadiazole (FBT), or benzo[1,2,5]thiadiazole (BT) electron acceptor (A) units, and either thiophene, 5-hexyl-2,2'-bithiophene, or benzofuran electron-rich end-caps (D'). These molecules are evaluated for their lowest energy conformations, in the gas phase, and rotational barriers are determined using electronic structure modeling. Subsequent NBO analysis is used to deconvolute the important intramolecular interactions, which determine geometric and conformational preferences. As described in more detail below, NBO analysis provides a method to analyze the types of interactions that occur through orbital overlap within a molecular structure and has yet to receive widespread use in studying the intramolecular contributions to conformational preferences. We will primarily use the analysis to show that there are through-space interactions that occur between lone

pairs of electrons and nearby empty orbitals. We are also able to separate the interactions into ones that provide stabilization and those that do not. We will also examine steric hindrance between two nearby filled orbitals and electrostatic interactions within a particular conformer. These types of analyses allow us to provide unique insight into the contribution of different intramolecular effects in determining the conformational preferences for the molecules studied here and more broadly to previous literature precedence. These efforts seek to provide a template for defining functional groups that can yield predictive capabilities for controlling shape in organic optoelectronic materials.

NBO ANALYSIS AS A TOOL FOR RESOLVING INTERACTIONS

Before we examine in detail the structures in Figure 1, it is worth highlighting relevant points on our approach to using the NBO analysis and on the challenges for addressing the multiple interactions between two chromophore fragments. In our computational study we rely primarily on the energetics of the underlying potential energy surfaces (PESs) obtained using electronic structure techniques as outlined in the Methods section. Examination of the emerging trends and deconvolution of energetics into the dominating interactions is provided by the NBO analysis, a well-established procedure previously described.⁴⁴ Notably, its application to the study of interactions between two π -conjugated heterocycles connected by a single bond is nontrivial due to the crowded interaction environment and delocalization of π -electrons. As a point of discussion, parts a and b of Figure 2 provide two molecular units connected by a

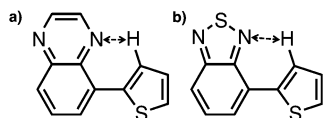


Figure 2. (a) Benzopyrazine + thiophene. (b) Benzo[1,2,5]thiadiazole + thiophene.

single bond (the benzopyrazine and benzo[1,2,5]thiadiazole connected to the thiophene). Molecule b has a stable planar configuration, which has been previously rationalized by a conformational “lock” due to a strong attractive N–H interaction.⁴⁰ However, this picture of a single dominating interaction does not hold for molecule a: DFT calculations show that the dihedral angle prefers to be twisted 30° from a planar configuration with an energy difference of approximately 0.4 kcal/mol. Note that the calculated N–H distances for the molecules a and b differ by 0.1 Å from each other and from the “equilibrium distance” proposed in ref 40. These differences suggest the existence of other interactions that need to be accounted for and analyzed to understand the PESs as a function of dihedral angle.

We now provide a brief description of the postprocessing of the standard NBO analysis. The goal is to identify the interactions between molecular fragments that give rise to the preference in rotamers and thereby the conformational preferences. We also define terms used in the subsequent discussion. The NBO analysis uses the second-order perturbation energies to evaluate donor–acceptor orbital interactions. These orbital interactions are defined as a delocalization of electrons from a filled orbital (σ and π bonds or lone pair of electrons) into a nearby empty orbital (such as σ^* and π^* orbitals). The

strongest interactions are mediated through the bridging atoms, i.e., the two atoms connected by the central single bond. The corresponding molecular fragment shown in green (Figure 5) includes these two atoms and the four near-bridge bonds. We define this fragment as “near-bridge bonds”. There are three types of orbital interactions important for this group. The first involves core electrons on the bridging atoms. Because of the symmetry with respect to the dihedral inversion, this group gives a small contribution to energy difference between the two rotamers, ΔE_{rot} . The other two types involve π - and σ -bonds. The contribution of donor–acceptor π -interactions toward ΔE_{rot} is overestimated because only the dominant Lewis structure is considered. This simplification is acceptable for conjugated molecules involving heteroatoms, and such molecules are in the focus of the present study. When all three types of orbital interactions are summed up, the result gives the interaction energy between the “near-bridge bonds” molecular fragments. The dominant contribution to the conformational preference is due to $\pi-\pi^*$ donor–acceptor interaction. The asymmetry between the two rotamers is caused by small variations of the π -bond order between the bridging atoms, as a several percent decrease in the bond order leads to an increase in the rotamer energy.

The other molecular fragments are associated with close-contact pairs of atoms (red and blue in Figure 5). The essential orbital interactions involve σ -bonds and sp^2 lone pairs as the donor components. Attractive donor–acceptor interactions are always canceled by strong steric repulsion that is typical for hybridized atomic orbitals, in contrast to pure p-orbitals which show strong donor–acceptor secondary bonding for both π - and σ -bonds.⁴⁵ It is important to note that the term steric repulsion used here is another term for the steric exchange energy, from the Pauli exclusion principle, that is outlined in the NBO literature. Therefore, the dominant forces in this group are steric repulsion and electrostatic attraction/repulsion. The rest of the individual orbital interactions are weaker than 0.5 kcal/mol. Comparison of ΔE_{rot} calculated from the sum of the interaction energies between the above-described molecular fragments with the energy obtained by DFT calculations is shown in Figure 3a. Evidently, the proposed NBO analysis can be used for qualitative predictions of conformational preferences (the sign of ΔE_{rot} is predicted correctly for the whole test set), unless the absolute value of ΔE_{rot} is much smaller than 1 kcal/mol (in that case DFT values cannot be trusted). In particular, the ΔE_{rot} of the mentioned benzopyrazine+thiophene molecule is accurately reproduced (see BP+T in Table 2).

A key limitation for estimating the full interaction energy between two molecular fragments is due to inaccurate evaluation of the electrostatic component. In the current implementation of the NBO analysis,⁴⁴ the only available procedure for estimating this component is calculation of the electrostatic interaction between natural atomic charges. This approximation is acceptable for through-space interactions but invalid for through-molecule interactions. To mitigate this problem we introduce a dielectric screening as detailed in the Supporting Information and neglect the interaction between charges located on the opposite sides of the molecule.

Differential solvation energies (i.e., the differences in solvation energy between two alternative rotamers) depend mainly on the electrostatic interaction of the close-contact atoms, in full agreement with reference electronic structure calculations (see Figure 3b). Note that “vdw” (van der Waals) charges must be used here, which are the charges obtained by fitting the

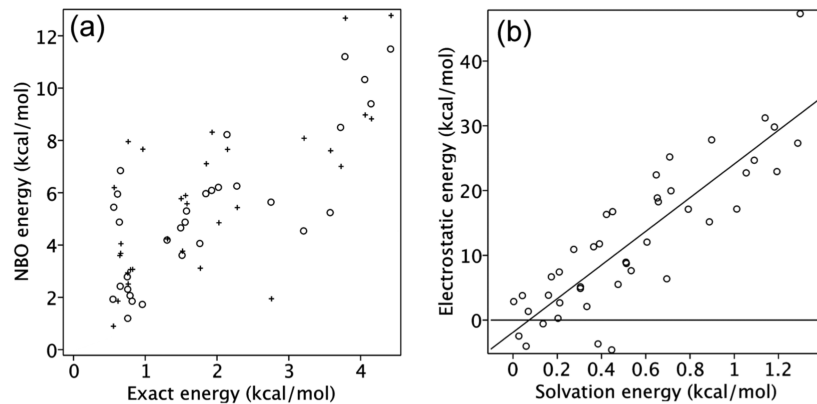


Figure 3. (a) Correlation between the ΔE_{rot} calculated as the sum of nonbonding interactions and the exact value (obtained from the reference ab initio calculations) for a set of 31 dihedrals (listed in the Supporting Information) having a single dominant Lewis structure; here circles mark the atomwise NBO analysis used in the paper and crosses mark the unitwise NBO analysis (\$DEL keyword in ref 44). (b) Correlation between the differential solvation energy and electrostatic energy of the close-contact atoms for a set of 44 dihedrals (listed in the Supporting Information).

electrostatic potential at the molecule surface. This is obtained by construction of the van der Waals molecular surface, as implemented in the Gaussian 09 package.

RESULTS AND DISCUSSION

General Perspective. We will examine the set of molecules in Figure 1 according to three subgroups that allow isolation of specific structural variations. These groups include (a) compounds **1–3**, which allow us to examine the differences between BT and PT, together with two variations of the pyridyl nitrogen regiochemistry; (b) compounds **4** and **5**, which provide an opportunity to consolidate the influence of PT regiochemistry with the same interior core as **1–3**, but with a different end group, i.e., benzofuran; and (c) compounds **6–8**, which provide significantly larger molecular systems wherein two FBT regiosomers are compared to a PT counterpart. For each section we compare the precise arrangement of atoms as determined by X-ray crystallography with the optimized geometries obtained through DFT. Despite the fact that the structures obtained through DFT are in the gas phase, we find excellent agreement between the calculated and experimentally determined structures, except for molecules **6** and **7**. These latter two provide relevant information on the influence of interactions in the crystal lattice and will be discussed more carefully in a subsequent section. RMS errors determined for molecules **1–5** and **8**, between the calculated and crystal structures, are 0.015 Å for bond lengths, 2.8° for dihedral angles, and 0.074 Å for nonbonded atomic distances.

In addition, dihedral intramolecular interactions (i.e., donor–acceptor orbital, steric, and electrostatic interactions) have been evaluated using the NBO program following the concepts outlined in the previous section. Since there are little to no differences in the magnitudes of the interactions between the fragments and the full molecules, the NBO analysis is performed for each smallest molecular fragment present in compounds in Figure 1, which are labeled as shown in Figure 4. The obtained results are summarized in Tables 1 (charges) and 2 (interaction energies), which will be extensively used in the subsequent discussion.

Influence of the Pyridyl Nitrogen. Molecules **1–3** (Figure 1) are compared to identify the role of the pyridyl nitrogen in mediating conformational preferences. The PT fragment is varied so that the pyridyl nitrogen was proximal (**1**) or distal (**2**) from the DTS core. Molecule **3** has a BT unit,

Table 1. NBO (natural) and “vdw” Atomic Charges for Heteroatoms Present in Molecules 1–8^a

atom	molecule	NBO	vdw
thiadiazole N	PT+T	-0.63	-0.4
pyridyl N	PT+T	-0.47	-0.5
F	FBT+T	-0.33	-0.2
O	PT+BF	-0.44	-0.3
thiophene S	PT+T	+0.51	0
thiadiazole S	PT+T	+0.95	+0.4

^aCharges are calculated for the representative small molecules from Figure 4. For the NBO charges, the full molecule values are provided in Tables S5 and S6 and Figure S4 (Supporting Information). All geometries have been optimized at the CAM-B3LYP/6-31G** level.

where the pyridyl nitrogen is replaced with a carbon–hydrogen bond. Figure 7a shows that the computed optimized molecular geometries adopt a nearly planar conformation. Quite significantly, this planar preference and overall molecular metrical parameters are very similar to those observed for the molecules via single crystal X-ray diffraction studies (see Figure 7b). Note that the crystal structures for compounds **1** and **3** show evidence of other conformations in the crystal (displayed by the dots in Figure 7b), which contribute to disorder in the lattice. Both crystals have a portion of structures with inverted, or flipped, thiophene (i.e., D' in the overall D–A–D–A–D' architecture) conformations as well as the optimized geometry conformation. Causes of this inverted D' unit will be evaluated below.

Rotational barriers for the different bonds in molecules **1–3** have been evaluated as follows. First, the dihedral angle between the DTS core unit and the adjacent acceptor unit is rotated from the optimized 0° to the inverted 180° at 20° intervals, as shown by the highlighted bonds in Figure 8. Both bonds on either side of the DTS are rotated simultaneously. The differences in the energy between the optimized structure and the structures with the different dihedral angles are plotted as a function of the dihedral angle in Figure 8a. The difference in energy between the preferred 0° conformation and the 180° conformation for molecule **1** is 2.9 kcal/mol (1.45 kcal/mol/dihedral), which is almost double the differences in molecules **2** and **3**, both being at 1.6 kcal/mol (0.8 kcal/mol/dihedral).

Rotational barriers for the dihedral angle between the PT or BT units and thiophene end group have been evaluated as well

Table 2. NBO Analysis of Across Dihedral Interaction Energies (in kcal/mol) for All Dihedrals Relevant to Molecules 1–8 (Figure 1)^a

molec	absolute interaction energies for cc atoms										differential energies		
	basic conformation (as shown in Figure 4)					inverted rotamer							
	pair	DA	+EX	ES	total	pair	DA	+EX	ES	total	cc	nbb	total
PT+T	TN-H	-3.9	1.5	-3.4	-1.9	TN-S	-3.7	2.4	-6.4	-4.0	-0.1	5.0	4.9
	PN-S	-3.0	1.5	-2.6	-1.1	PN-H	-1.9	2.3	-1.3	1.0			
dPT+T	TN-H	-4.5	1.9	-3.5	-1.6	TN-S	-2.3	1.8	-5.7	-3.9	-3.6	5.7	2.1
	H-S	-2.6	1.8	2.4	4.1	H-H	-1.1	1.8	1.0	2.8			
BT+T	TN-H	-4.5	2.1	-3.5	-1.3	TN-S	-2.9	2.3	-6.2	-3.9	-3.0	4.9	1.9
	H-S	-2.6	2.0	1.4	3.4	H-H	-1.3	1.9	1.0	3.0			
PT+BF	TN-H	-3.5	1.3	-2.7	-1.4	TN-O	-1.3	1.4	1.1	2.5	4.0	2.9	6.8
	PN-O	-0.5	1.8	-1.0	0.8	PN-H	-1.2	1.7	-0.9	0.8			
dPT+BF	TN-H	-3.0	1.1	-2.4	-1.3	TN-O	-0.5	0.9	0.8	1.7	3.7	7.5	11.2
	H-O	-1.2	2.2	-1.3	0.9	H-H	-0.6	1.1	0.5	1.7			
FBT+T	TN-H	-5.6	2.6	-3.8	-1.2	TN-S	-4.9	4.1	-6.9	-2.8	-1.9	3.1	1.2
	F-S	-4.8	3.2	-1.6	1.5	F-H	-4.3	3.2	-1.9	1.3			
dFBT+T	TN-H	-4.8	2.0	-3.6	-1.6	TN-S	-3.2	2.5	-6.4	-3.9	-2.3	5.1	2.8
	H-S	-2.6	1.8	1.1	2.9	H-H	-1.4	1.9	1.1	3.0			
BP+T	N-H	-2.8	2.8	-1.3	1.5	N-S	-5.1	3.6	-3.5	0.1	-0.9	0.7	-0.3
	H-S	-2.0	1.9	1.4	3.2	H-H	-1.6	2.6	1.1	3.7			
T+T	S-H	-0.9	0.4	0.4	0.8	S-S	-0.9	0.1	2.6	2.6	2.0	2.9	4.9
	H-S	-0.9	0.4	0.4	0.8	H-H	-0.7	0.2	0.7	0.8			

^aThe labeling for the fragments used in the analysis is given in Figure 4 (also, BP+T is the molecule shown in Figure 2a, and T+T is bithiophene). The labeling of interaction groups (cc and nbb) is shown in Figure 5. Other notations: “pair” means a pair of close-contact atoms (PN = pyridyl N, TN = thiadiazole N) for which the absolute interaction energies are given, including the donor–acceptor orbital interaction energy between lone pair of electrons in heteroatoms and adjacent empty orbitals (“DA”), its sum with the steric (exchange) energy (“+EX”), the electrostatic energy (“ES”), and the total interaction energy. All geometries have been optimized at the CAM-B3LYP/6-31G** level. The strongest donor–acceptor orbital interactions are visualized in Figure 6.

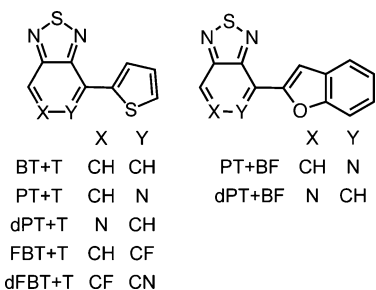


Figure 4. Molecular fragments present in molecules 1–8 (Figure 1) and notations for the dihedrals subjected to the NBO analysis, the results of which are summarized in Tables 1 and 2

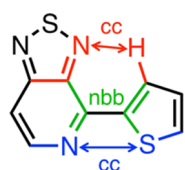


Figure 5. Example of the near-bridge bonds (nbb) and close contact (cc) interactions.

(Figure 8b) using the same procedure for computing the rotational barriers outlined above. We observe the same general trend for the rotational barriers seen in Figure 8a. Molecule **2** has the highest 180°, or inverted D', conformation energy difference at 2.8 kcal/mol (1.4 kcal/mol/dihedral). This value is comparable with the 180° conformation of molecule **1** in Figure 8a, as both values reflect a preference for the pyridyl nitrogen in close proximity to sulfur. Molecules **1** and **3** have

smaller inverted D' conformational energies than **2**, with a difference of 1.7 kcal/mol for both dihedrals.

It was of interest to us to determine the shape and overall angle of the molecules, since these parameters are known to influence the crystallization and solid-state packing.³⁰ In our studies, molecular angles are represented by using the angle from the centroid of the thiophene ring to the silicon of the core DTS unit to the other end thiophene ring centroid. Molecule **1** has the smallest molecular angle at 115.2°, and molecule **3** has the largest molecular angle at 121.2°. To understand the difference between the dihedral PT+T and the other two structures, dPT+T and BT+T (see Figure 4 for notations), we refer to the NBO analysis summarized in Table 2. We see that the presence of nitrogen atom in the near-bridge bonds strengthens the corresponding donor–acceptor interaction (the first nbb column). In addition, the electrostatic N–S attraction in PT+T is changed to H–S repulsion in dPT+T and BT+T. The sum of these two factors explains the steep curve for the PT+T dihedral in Figure 8. In ΔE_{rot} , the contribution of the near-bridge bonds is nearly the same (the second nbb column), whereas the net effect of the interaction between the close-contact atoms is negative (cc column). This explains the difference between the relative energies at 180° in Figure 8.

At this point we note that for compounds **1**–**3** there is an excellent agreement between conformations in the solid state and the theoretically determined lowest energy conformation in the gas phase. The relative energies of the different conformers have been determined, i.e. at 0° and 180° in Figure 8. Since these values for molecules **1** and **3** are comparable to kT at room temperature (i.e., smaller than 1 kcal/mol), it is not surprising that we observe contributions from inverted thiophene end groups in the crystal structures.

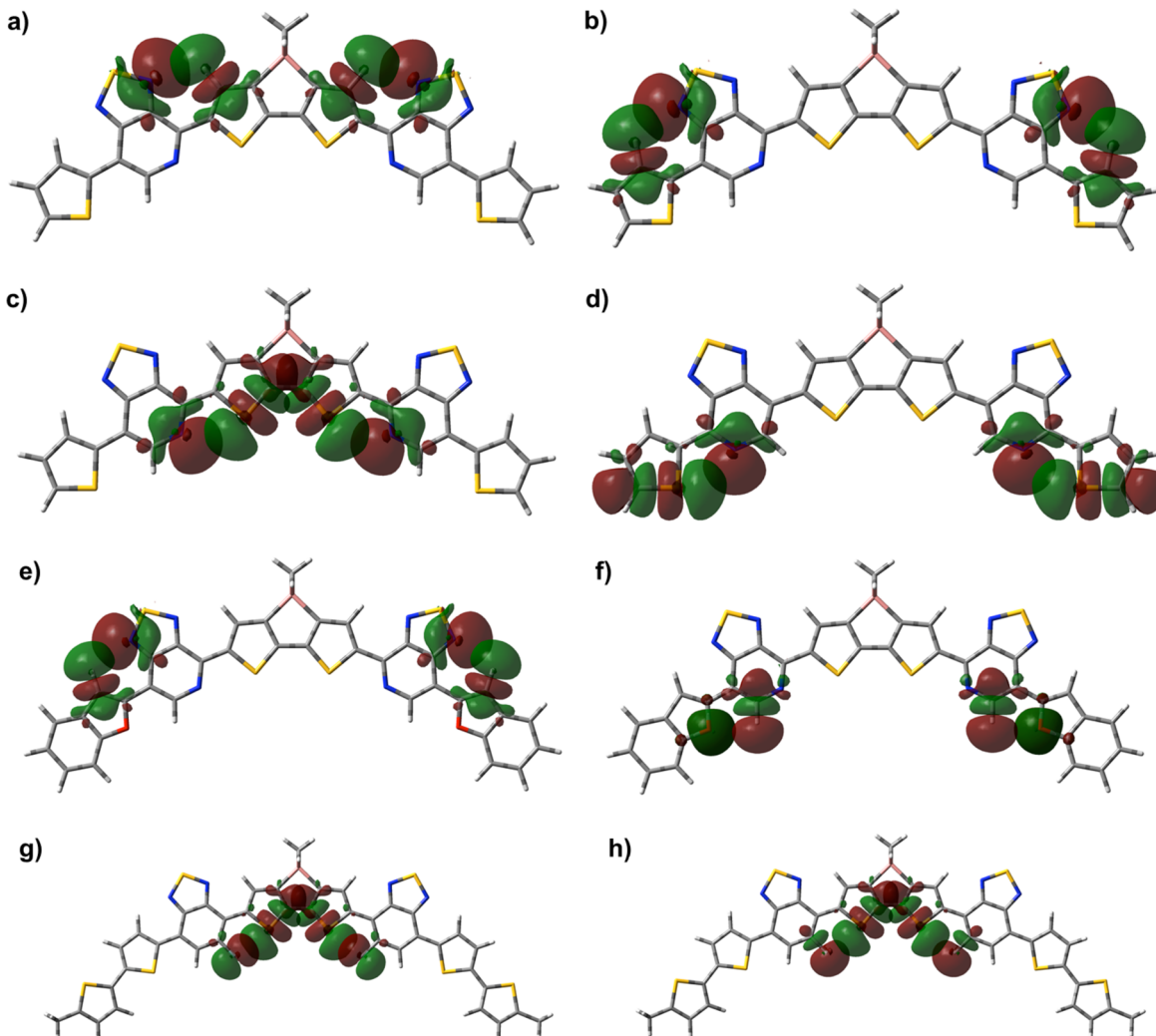


Figure 6. Visualization of the strongest donor–acceptor orbital interactions mediated through close-contact atoms: (a, b) thiadiazole nitrogen to hydrogen in molecule **1** (TN–H in PT+T and dPT+T in Table 2); (c, d) pyridyl nitrogen to sulfur in molecules **1** and **2** (PN–S in PT+T and dPT+T); (e) thiadiazole nitrogen to hydrogen in molecule **5** (TN–H in dPT+BF); (f) oxygen to hydrogen in molecule **5** (H–O in dPT+BF); (g, h) fluorine to sulfur in molecule **6** (F–S in FBT+T). For all the listed close-contact pairs, the donor is a lone pair on the first atom (there are two of them for fluorine) and the acceptor is a σ^* antibonding orbital involving the second listed atom (there are two of them for sulfur and oxygen; in this case, the strongest interaction is visualized).

End Donor Effects. Molecules **4** and **5** were previously investigated to understand how differences in bulk morphology may be related to molecular shapes/angles.³⁰ In order to rationalize this difference in molecular shape, the intramolecular interactions have been evaluated in the same way as for molecules **1–3**. Optimized geometries show a planar structure (Figure 9a). There is evidence in the crystal structure of compound **4** for an inverted benzofuran end group, as shown by the dotted atom sites in Figure 9b. A rationalization for this conformation will be discussed below.

Figure 10 shows calculated rotational barriers for molecules **4** and **5**. First, we will look at the rotation of the bond between the DTS and PT units (Figure 10a), where there is a clear difference in the rotational barriers, similar to what is observed in Figure 8a. Molecule **5** has a larger 180° conformation energy than molecule **4**, with energies of 3.0 and 1.6 kcal/mol, respectively. Figure 10b shows an analogous curve for the rotation of the bond between PT and benzofuran. The potential energy curves for molecules **4** and **5** are nearly the same up to 120°. The relationship between the dihedral angle and energy for

molecule **5** is different from what is observed in the other molecules insofar as there is a nearly flat energy level from 140° to 180°, and the exact cause of this is not entirely clear. Ultimately, the relative energy of the 180° conformation for molecule **5** is the highest for all the compounds in the study, at 8.3 kcal/mol, or 4.15 kcal/mol/dihedral. This could be an indication as to why there is no other conformer observed in the crystal structure for molecule **5** besides the lowest energy conformer. The low energy difference between the optimized and inverted benzofuran for compound **4**, 1.0 kcal/mol (0.5 kcal/mol/dihedral), is consistent with the observation of an inverted benzofuran conformation in the crystal structure.

The molecular angles for compounds **4** and **5** have been measured as the angle between the centroids of the benzene rings of the benzofurans and the silicon atom of the DTS. Molecules **4** and **5** have angles of 117.9° and 114.1°, respectively. They show the same trend as molecules **1** and **2**, namely, when the pyridyl N is proximal to the DTS sulfur, the molecular angle becomes smaller. It was shown by Welch et al. that these differences in molecular angle have an effect on the order of

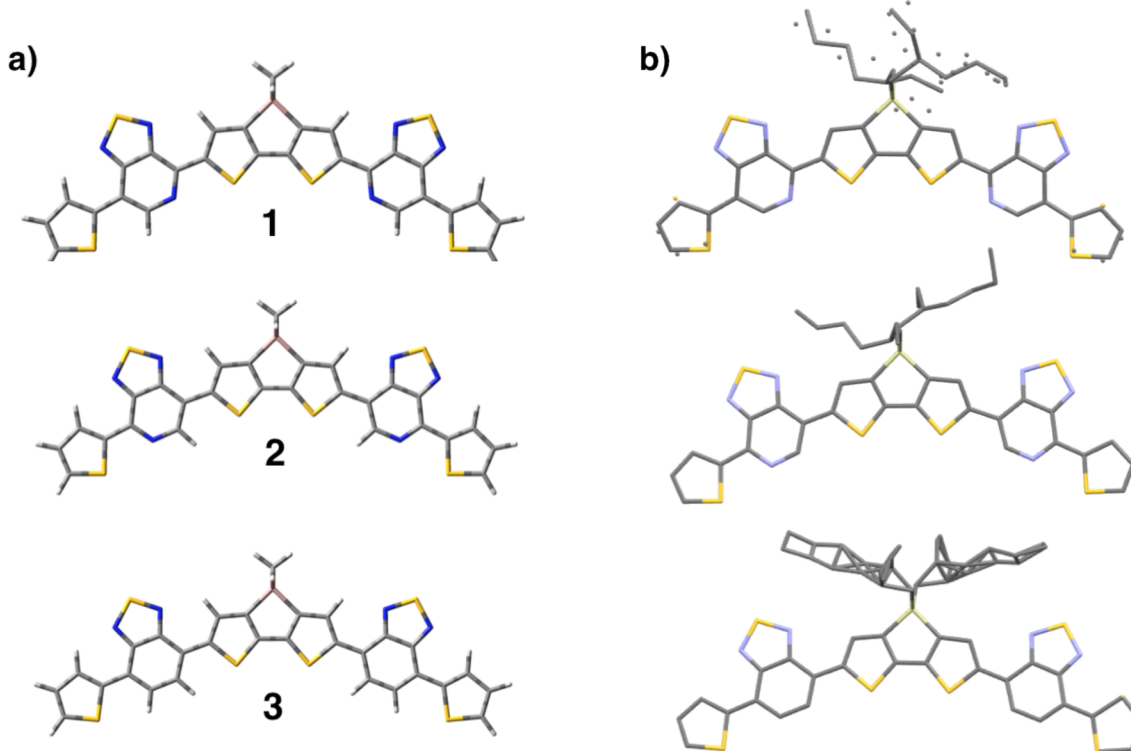


Figure 7. Comparison of the (a) optimized geometries of molecules **1**–**3** using the CAM-B3LYP/6-31G** level (in vacuum) and (b) the crystallographically determined structures (gray = carbon, blue = nitrogen, yellow = sulfur, pink = silicon, white = hydrogen). The hydrogens were removed from the crystal structures for clarity. The alkyl chains shown are a mixture of the *R* and *S* isomers, and the crystal structures for **1** and **3** show evidence of different rotamers for the end thiophene.

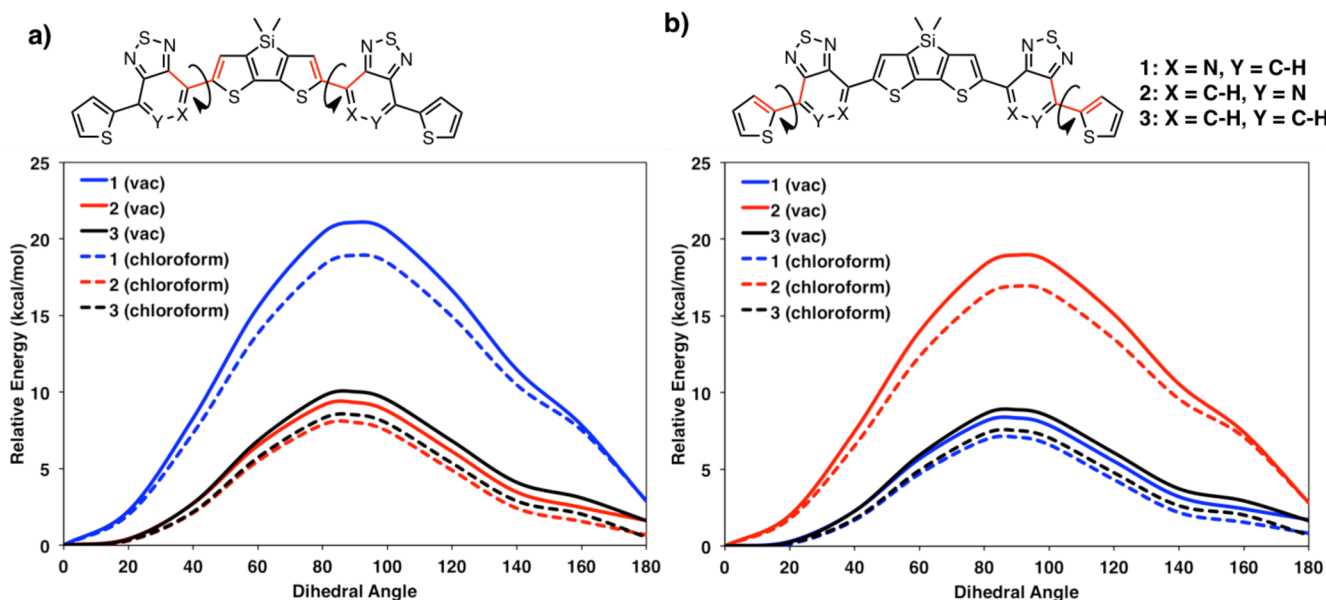


Figure 8. Energetic barriers of molecules **1**–**3** for (a) the rotation of the bond between the PT/BT and the DTS units and (b) the rotation of the bond between the PT/BT and the thiophene units. Calculations were performed in both vacuum (solid lines) and chloroform (dashed lines). The optimized geometry is denoted by the 0° dihedral angle. Both dihedrals are rotated simultaneously in the same direction.

these molecules in the solid state, with important consequences on the performance of these molecular semiconductors in optoelectronic devices.³⁰

To understand the “plateau” of the relative energy in the 120°–180° range for dPT+BF in Figure 10b, we refer to the NBO analysis in Table 2. It shows that in the inverted conformation both TN–O and H–H electrostatic interactions are

repulsive, leading to a nonplanar geometry similar to the T+T dihedral. In the lowest energy conformation both TN–H and H–O electrostatic interactions are attractive and thereby contribute to the large value of ΔE_{rot} .

FBT Regioisomers. Molecule **6** is a well-known high-performing small molecule for OPV applications.¹⁰ We were interested to see if the fluorine on the FBT acceptor would

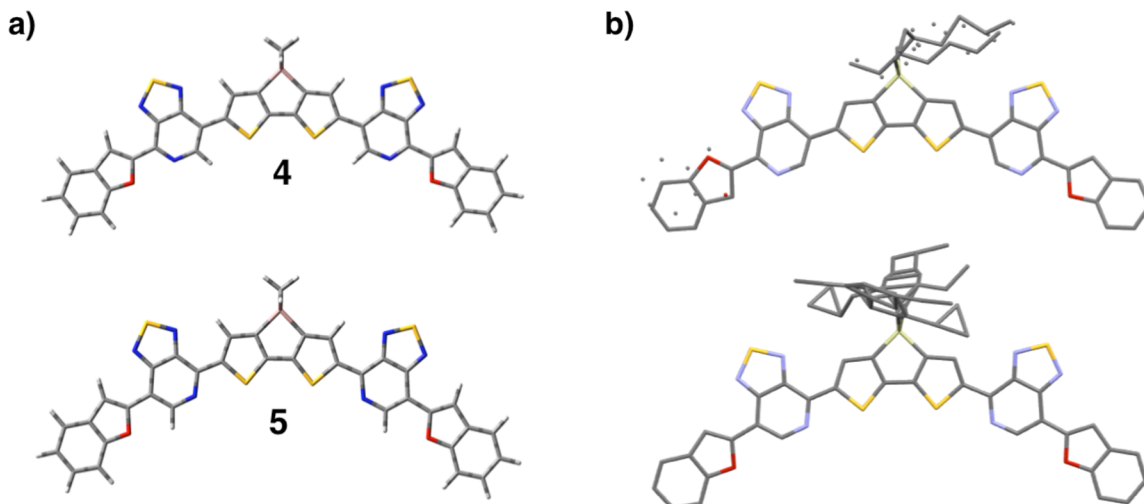


Figure 9. Comparison of the (a) optimized geometries of molecules **4** and **5** using CAM-B3LYP/6-31G** (in vacuum) and (b) the crystallographically determined structures (gray = carbon, blue = nitrogen, yellow = sulfur, pink and light green = silicon, white = hydrogen). The hydrogens were removed from the crystal structures for clarity. The alkyl chains shown are a mixture of the *R* and *S* isomers and the crystal structures for **4** show evidence of different rotamers for the end benzofuran.

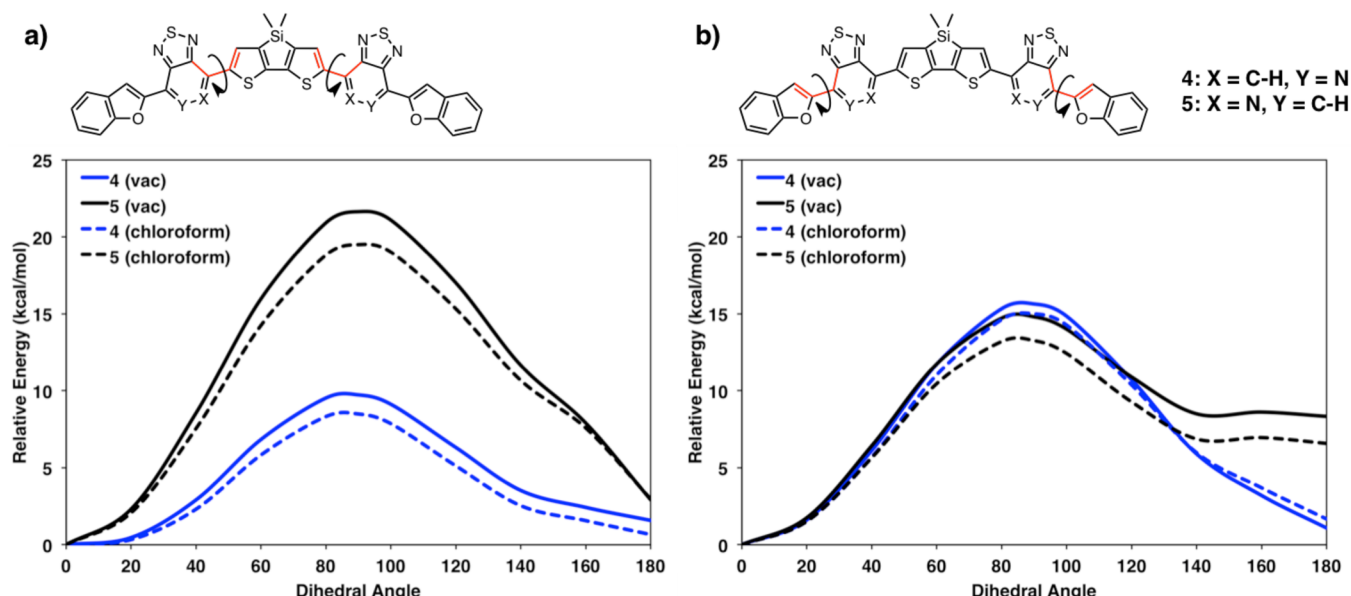


Figure 10. Energetic barriers of molecules **4** and **5** for (a) the rotation of the bond between the PT and the DTS units and (b) the rotation of the bond between the PT and the benzofuran units (see also Figure S5 of the Supporting Information for a finer-grid version of the curve **5**). Calculations were performed in both vacuum (solid lines) and chloroform (dashed lines). The optimized geometry is denoted by the 0° dihedral angle. Both dihedrals were rotated simultaneously in the same direction.

display any of the trends for maintaining molecular shape and intramolecular interactions as described for the PT-containing molecules. Therefore, two FBT regiosomers (compounds **6** and **7**) were analyzed for intramolecular interactions and were compared with the properties of molecule **8**, which provides a nearly isostructural PT-containing counterpart.¹³ The optimized geometries for molecules **6–8** show a mostly planar structure with only the dihedral between the thiophene end units not at 180° (Figure 11a).

The lowest energy conformation for **6** is not the conformation displayed in the crystal structure, shown in Figure 11. The crystal lattice conformation contains a flipped dihedral between the DTS core and the FBT acceptor. We will investigate this discrepancy further below. Molecule **7** displays two

polymorphs in the crystal lattice. One polymorph has the same conformation as the calculated lowest energy conformation, while the other displays the same flipped dihedral as the crystal conformation of molecule **6**. These differences could be due to factors that are beyond the scope of this work and are not intrinsic to the molecular structure that mediates the crystallization process, for instance, aggregation in solution or the more complex balancing of intermolecular distances and orientations for minimizing lattice energies. Molecule **8** has the same lattice conformation as the calculated optimized geometry, which is not surprising since it has the same units as the previously described molecules **1–5**.

The rotational barriers for molecules **6** and **7** do not show any significant differences based on whether the fluorine is

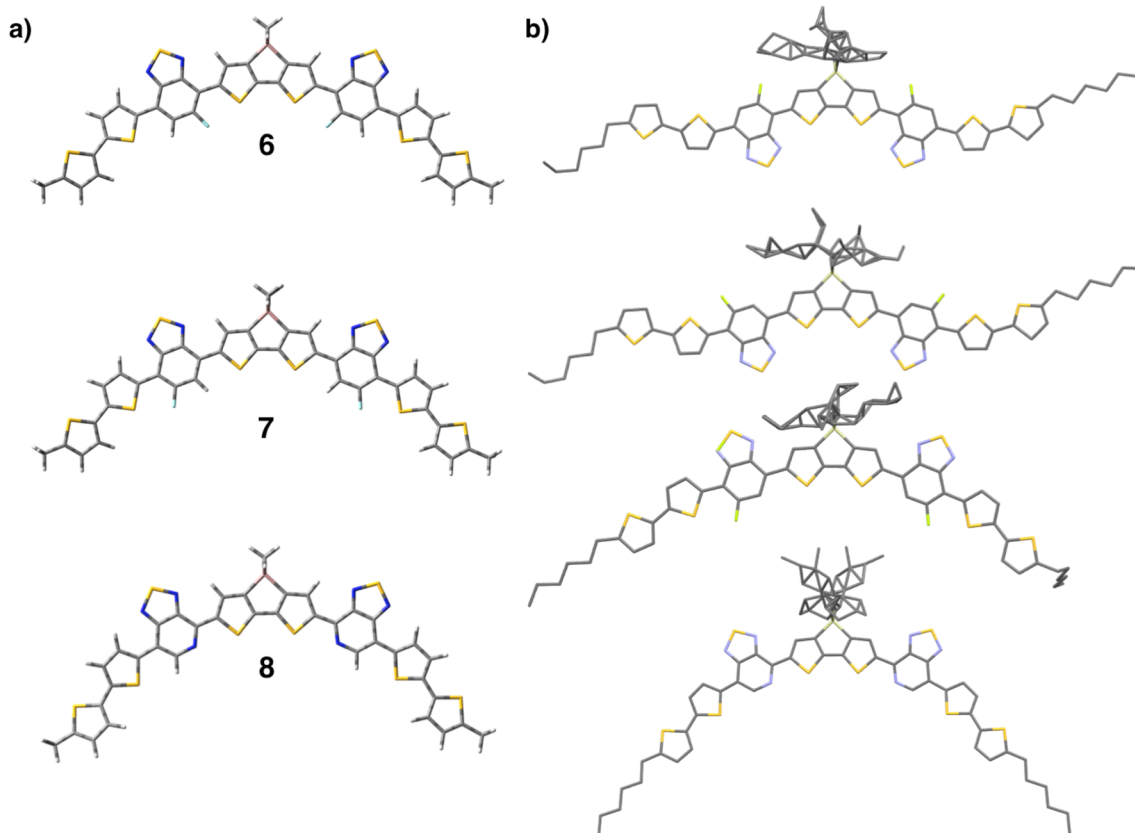


Figure 11. Comparison of the (a) optimized geometries of molecules **6–8** using CAM-B3LYP/6-31G** (in vacuum) and (b) the crystallographically determined structures (gray = carbon, blue = nitrogen, yellow = sulfur, pink and light green = silicon, white = hydrogen). The hydrogens were removed from the crystal structures for clarity. The alkyl chains shown are a mixture of the R and S isomers and the crystal structures for **7** are the two different polymorphs obtained.

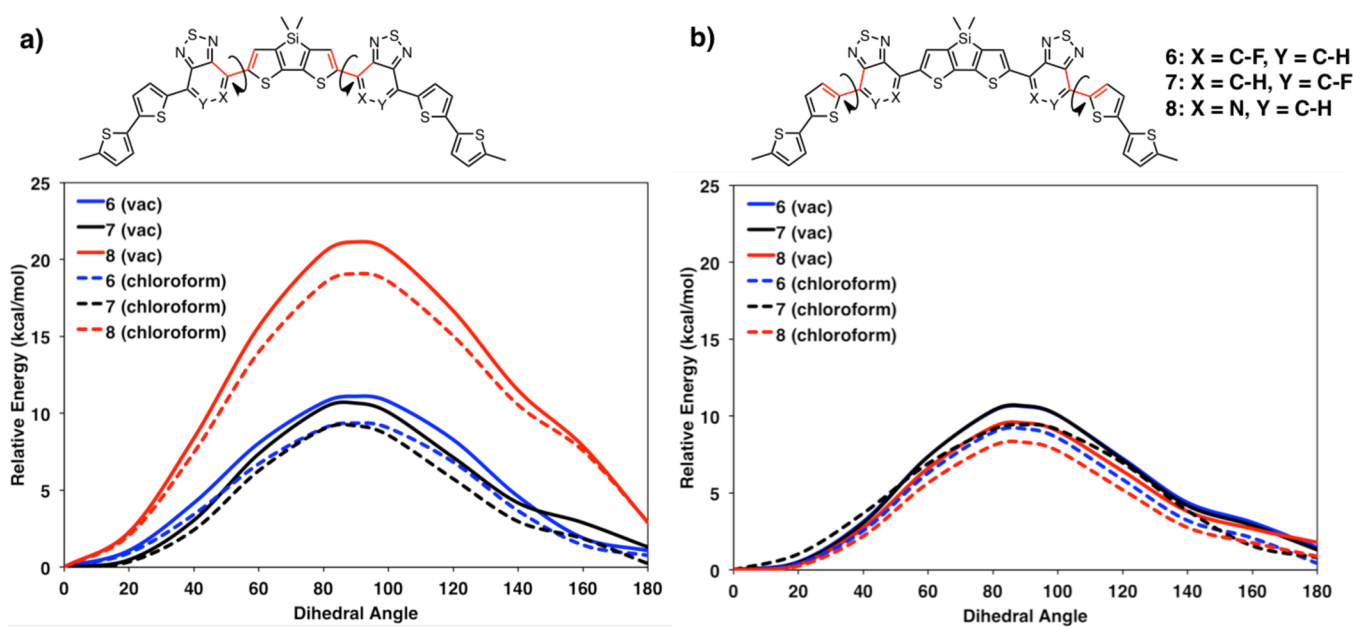


Figure 12. Energetic barriers of molecules **6–8** for (a) the rotation of the bond between the PT/FBT and the DTS units and (b) the rotation of the bond between the PT/FBT and the thiophene units. Calculations were performed in both vacuum (solid lines) and chloroform (dashed lines). The optimized geometry is denoted by the 0° dihedral angle. Both dihedrals were rotated simultaneously in the same direction.

proximal or distal to the DTS core (Figure 12). The difference between the 0° and 180° conformations when the DTS–acceptor bonds are rotated for molecule **6** is only 1.3 kcal/mol.

This value is low compared to compound **8**, with a 3.0 kcal/mol difference for both dihedrals (Figure 12a). Molecule **7** also has a small difference (1.3 kcal/mol) between the optimized and

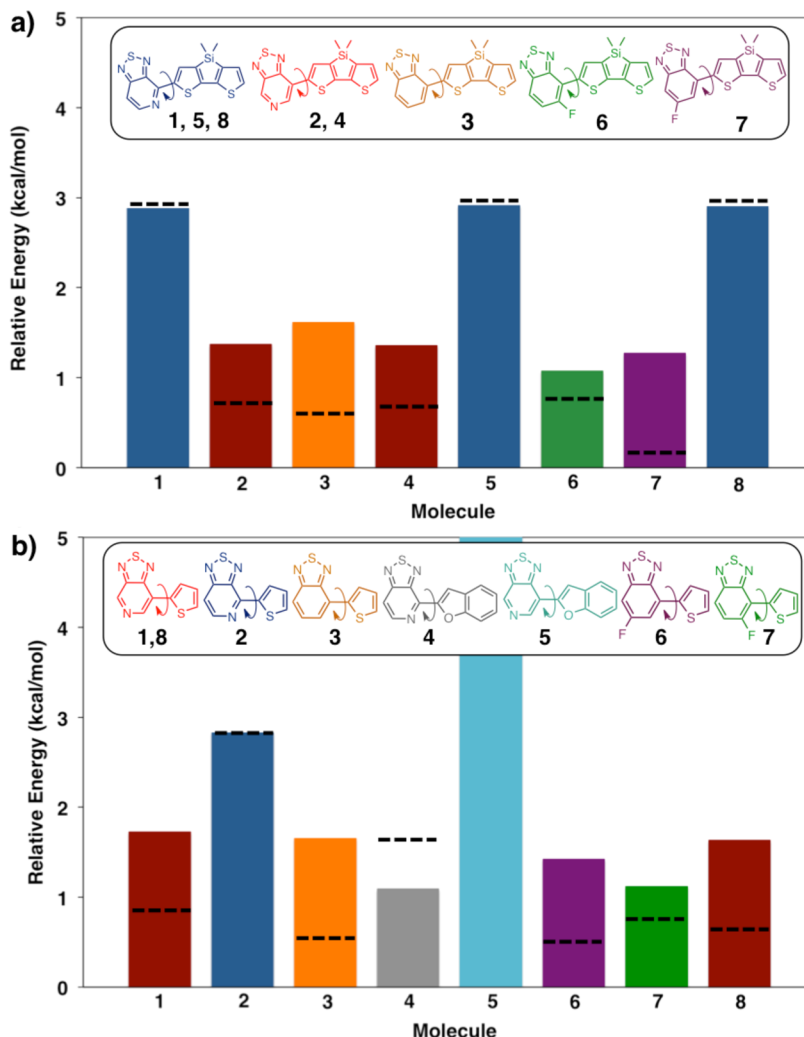


Figure 13. Double ΔE_{rot} values (i.e., for the case when two symmetry-equivalent dihedrals are inverted) for (a) the dihedral between the core and the acceptor ($D-A$) and (b) the dihedral between the acceptor and the end group ($A-D'$). The solid bars and dashed lines refer to the calculations in vacuum and chloroform, respectively. The values for molecule 5 in part b are 7.6 kcal/mol in vacuum and 5.9 kcal/mol in chloroform.

inverted conformations. The low rotational barriers are entirely consistent with the inverted conformations in the crystal structures of compound 6 and one of the polymorphs of molecule 7. For the rotation of the bond between the acceptor units and the thiophene, there are no differences between the three molecules (Figure 12b). All three molecules show a difference in energy between the 0° and 180° conformations of 1.3–1.8 kcal/mol for the rotation of both dihedrals. Our results agree with previous analysis of the same low rotational barrier trends with a similar molecule containing a fluorinated BT acceptor.⁴⁰

Molecular angles have been measured between the centroid of the furthest thiophene and the silicon atom of the DTS core. There is also no clear trend in the differences in the molecular angles between molecules 6 and 7. In fact, compound 6 has a larger molecular angle (123.4°) than compound 7 (121.6°), and both have a much larger molecular angle than molecule 8 (115.2°). The NBO analysis is fully consistent with ab initio calculations: all the dihedrals dPT+T, BT+T, dFBT+T, and FBT+T have very similar interaction patterns. The only difference is that in FBT+T the F–S and F–H interactions are much less repulsive than the corresponding H–S and H–H interactions in the first three molecules, resulting in a planar geometry.

The anticipated attraction between fluorine and sulfur/hydrogen is turned to a weak repulsion by strong steric effects, and both F–S and F–H distances are smaller than the “equilibrium” values previously proposed.⁴⁰

Comparison of the Heterotomic Interactions across the Molecular Family. Figure 13 provides a summary of the most relevant structures and the difference in rotamer/conformational energies. Note also that examination of Figures 7, 9, and 11 shows that the rotational barriers do not exceed 10 kcal/mol per dihedral. According to transition state theory,⁴⁶ every 5 kcal/mol increases the overbarrier transition time by a factor of 1000 at room temperature with a picosecond prefactor (related to characteristic time scale for vibrations). Thus, the conformations of 1–8 are thermally equilibrated in a solution within nano- to milliseconds time scales. The calculated energies required to planarize the conjugated backbone are within tenths of kilocalories/mole and are distributed among four to six dihedrals. Therefore, the only energy parameter important in a discussion of conformational preferences is the ΔE_{rot} between different rotamers.

The trend in Figure 13 can be rationalized using the NBO analysis data shown in Table 2. The first important observation to be made is that, for all the dihedrals discussed so far, the

dominant contribution to ΔE_{rot} originates from the interactions of the near-bridge bonds (more specifically from donor–acceptor interactions among the π -systems of the two molecular units). This interaction is particularly strong when one unit is an electron donor and another one is an acceptor. From our NBO analysis a simple rule of thumb has emerged: the π -systems of the two molecular units prefer their double bonds to be in the trans conformation. This rule requires the proper Lewis structure to be guessed, which is trivial for **1–8**. In cases when the choice of the Lewis structure is ambiguous (e.g., for the BP+T molecule shown in Figure 2a), how this π -contribution contributes to rotamer preferences becomes less convenient as a predictive tool.

The interplay between near-bridge bonds and close-contact interactions produces the variety of ΔE_{rot} values provided in Figure 13. For the PT+T dihedral (dark blue color in Figure 13), the symmetric position of the two nitrogen atoms and the same-sign charge of the sulfur and hydrogen results in a small difference between the alternative rotamers (see Figure 13a,b); therefore, the ~ 3 kcal/mol difference in Figure 13 arises from more favorable near-bridge bond interactions in the lowest energy conformation. For the dPT+BF combination, conformational preference occurs primarily in accordance with electrostatic preferences (see Figure 14c,d). Those two interactions

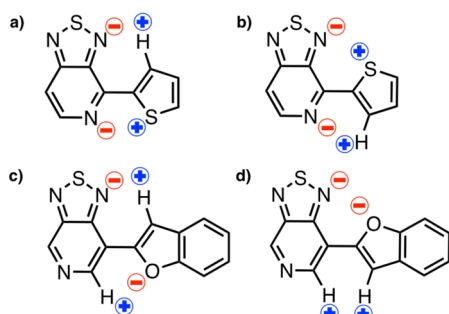


Figure 14. Representative charges on PT+T and dPT+BF: (a and c) lowest energy conformations and (b and d) inverted conformers.

show the strongest preference and therefore create some of the strongest conformational “locks” in this study. For other dihedrals, the close-contact interactions counteract with the interactions of the near-bridge bonds, lowering the differential energy, so that alternative rotamers may coexist in solution and may be observed in a crystal environment. Upon solvation, the differential energy follows the trend dictated by the electrostatic interaction between close-contact atoms (see Figure 3b). For example, the nearly symmetric charge distribution in PT+T molecule makes its ΔE_{rot} solvent-independent.

CONCLUSIONS

Eight molecular semiconductors with the D’-A-D-A-D’ architecture were evaluated for conformational preferences in vacuo and in a simulated solvent environment. Using DFT methodology, bond-rotational barriers as well as rotamer energetics at stable configurations have been explored in detail. In particular, the computed optimal geometries of the compounds have been shown to be remarkably consistent with the metrical parameters obtained via single crystal X-ray diffraction studies. The heights of the calculated rotational barriers (several kcal/mol) ensure a good level of probability for the molecules to adopt the 0° or 180° rotamers in solution at room temperature.

The ΔE_{rot} between the inverted rotamers (i.e., conformers at dihedral angles of 0° and 180°) is an important parameter that influences the bulk organization of these materials in the solid state, particularly in active layers within optoelectronic devices.

To examine the relationship between the ΔE_{rot} determined by DFT and the molecular connectivity, we used NBO analysis, which qualitatively reveals relevant intramolecular interactions that influence the geometry and relative energy of the different rotamers. In the 8 molecules, 12 important dihedral rotations have been investigated in detail. It was determined that the angular dependence of the bond-rotational barriers and the ΔE_{rot} values cannot be satisfactorily described by a single parameter, or even by a single dominant interaction; instead, multiple competing interactions have been identified. Qualitatively, for each studied dihedral angle, there are three groups of interacting atoms: near-bridge bonds and two pairs of close-contact atoms aside the bridge. The contribution of the first group is dominant and originates mainly from π -bond donor–acceptor interactions. The asymmetry of this interaction with respect to the dihedral inversion originates from variations of the π -bond order between the bridging atoms and follows a simple empirical rule: the π -systems of the two molecular units prefer their double bonds to be in trans conformation, evidenced by the higher energy of the inverted conformation for all molecules studied. The close-contact interactions vary in strength and sign depending not only on the atoms in contact but also on their molecular environment. For this group, the strongest donor–acceptor interactions involve the delocalization of sp^2 lone pairs on heteroatoms into nearby σ^* -orbitals. Yet, steric repulsion dominates and, together with electrostatics, determines the interaction energy. For the molecular fragments considered here, nitrogen–sulfur interactions are always attractive and nitrogen–hydrogen interactions depend on the molecular environment, whereas fluorine and oxygen show no noticeable binding. When all constituent interactions have the same sign, a “conformational lock” occurs, which leads to a single preferred rotamer. Moreover, even though calculated at the single molecule level, the strength of these interactions is sufficient that one finds the preferred conformation within lattice constraints.

Finally, it is interesting to note that a greater preference for a given conformational isomer would result in an increased ability for the molecules to crystallize under kinetically constrained conditions, for example, when spin-cast from solution as part of a blend.¹⁶ Furthermore, when the ΔE_{rot} values are small, multiple rotamers are detected in the crystal structures, thus suggesting less ordered bulk molecular organization. By understanding the complex interplay of various interactions present, it should be possible to attach units in a way that maximizes these interactions and leads to “locked” structures, in effect pre-programming to some extent from the molecular connectivity the solid-state organization and the dynamics of crystallization.

METHODS

Computational Methods. Geometry optimizations were completed on small donor–acceptor molecules using both the density functional theory (DFT) and the Moller–Plesset perturbation theory (MP2) (Supporting Information). Rotational barriers were also computed using both DFT and MP2.^{47–49} DFT has been shown to overestimate rotational barriers;⁵⁰ however, our calculations have shown that the MP2 and DFT results have barriers of the same magnitude when the calculations are done using the basis set 6-31G** (Supporting Information). We have also shown that a sufficiently larger

MP2 basis set, cc-pVTZ, agrees quite well with the DFT results (Figure S2, Supporting Information).⁵¹ Since the full molecules have too many atoms to complete MP2 optimizations without the extra computational expense (and the comparison with DFT proved to not be substantially different), we used the DFT results in this paper. The functional CAM-B3LYP, with the basis set 6-31G**, was used for the geometry optimizations because it has been shown previously to accurately describe long-range properties of extended π -conjugated systems similar to those in this study.^{18,52,53} Calculations performed in chloroform were done using the conductor-like polarizable continuum model.⁵⁴ The alkyl chains in the molecules were replaced with methyl groups for all geometry optimizations. Rotational barriers were assessed by fixing the dihedral of interest, at 20° intervals. The 180° conformation was fixed at the appropriate dihedral and the rest of the molecule was allowed to relax. Intramolecular nonbonding interactions were assessed using the natural bond orbital analysis⁴⁴ (NBO version 5.9). All ab initio calculations are performed with the Gaussian09 software suite (Frisch, M. J., et al.; Gaussian, Inc., Wallingford, CT, 2009).

Experimental Methods. The syntheses of compounds **1**, **2**, and **7** are reported in the Supporting Information. Single crystal growth of **1** and **3** was completed by slow evaporation of a chloroform solution. Molecule **2** single crystals were grown by slow evaporation of a dichloromethane/benzene solution. For molecules **4**, **5**, **6**, and **8**, single crystal growth and characterization were previously reported.^{14,18,30} Crystals of **7** were grown by diffusing 2-butanone into a 1.5 mg/mL solution of **7** in thiophene through a 500 μm aperture at 4 °C. The polymorph of **7** was grown by diffusing 2-butanone into a 1.5 mg/mL solution of **7** in carbon disulfide through a 500 μm aperture at 4 °C.

Crystals of compounds **1–3** were mounted in Paratone oil on a glass fiber loop and placed on a Bruker Kappa Apex II ($\lambda = 0.71073 \text{ \AA}$, 50 kV/30 mA) at 100 K, with a fine focus sealed tube as the X-ray source. ω -Scans were collected with Bruker AXS APEX2 software. Crystals of compounds **6** and **7** were mounted in Paratone-N oil on a MiTeGen loop and put on a Bruker AXS APEXII diffractometer in station 11.3.1 of the Advance Light Source at Lawrence Berkeley National Laboratory, using monochromatic radiation ($\lambda = 0.7749 \text{ \AA}$) at 100 K. A sphere of data was collected with a scan width of 0.3° using Bruker AXS APEX2 software. Refinement of the collected data was completed as follows. The intensities were integrated and the Lorenz and polarization corrections applied using SAINT (Bruker AXS, Inc., Madison, WI, 2011). Absorption and volume corrections were made using SADABS (Sheldrick, G. M.; Bruker AXS, Inc., Madison, WI, 2008). The structure was solved in SHELXS-97 or SHELXS-2013 using direct methods and refined in SHELXL-97 or SHELXL-2013 using full-matrix least-squares on F2.⁵⁵

■ ASSOCIATED CONTENT

Supporting Information

Materials and methods, synthetic and spectroscopic details of **1–8**, single crystal X-ray diffraction, theoretical calculation details, and CIF files. This material is available free of charge via the Internet at <http://pubs.acs.org>.

■ AUTHOR INFORMATION

Corresponding Authors

*G.C.B. e-mail: bazan@chem.ucsb.edu.

*S.T. e-mail: serg@lanl.gov.

Present Address

[†]Department of Chemistry, Dalhousie University, Halifax, Nova Scotia, B3H 4R2, Canada.

Author Contributions

The manuscript was written through contributions of all authors. All authors have given approval to the final version of the manuscript.

Notes

The authors declare no competing financial interest.

■ ACKNOWLEDGMENTS

We acknowledge support for the synthesis of the materials and calculation efforts by the Center for Energy Efficient Materials (CEEM), an Energy Frontier Research Center funded by the U.S. Department of Energy (DOE), Office of Basic Energy Sciences (BES) (DE-DC0001009). We also acknowledge support of the Los Alamos Laboratory Directed Research and Development program. Los Alamos National Laboratory (LANL) is operated by Los Alamos National Security, LLC, for the National Nuclear Security Administration of the U.S. Department of Energy under contract DE-AC52-06NA25396. The Advanced Light Source is supported by the Director, Office of Science, Office of Basic Energy Sciences, of the U.S. Department of Energy under Contract No. DE-AC02-05CH11231.

■ REFERENCES

- (1) Brabec, C.; Scherf, U.; Dyakonov, V. *Organic Photovoltaics: Materials, Device Physics, and Manufacturing Technologies*; Wiley: New York, 2011.
- (2) Gendron, D.; Leclerc, M. New Conjugated Polymers for Plastic Solar Cells. *Energy Environ. Sci.* **2011**, *4*, 1225–1237.
- (3) Veinot, J. G. C.; Marks, T. J. Toward the Ideal Organic Light-Emitting Diode. The Versatility and Utility of Interfacial Tailoring by Cross-Linked Siloxane Interlayers. *Acc. Chem. Res.* **2005**, *38*, 632–643.
- (4) Brunetti, F. G.; Kumar, R.; Wudl, F. Organic Electronics from Perylene to Organic Photovoltaics: Painting a brief history with a broad brush. *J. Mater. Chem.* **2010**, *20*, 2934–2948.
- (5) Mishra, A.; Bäuerle, P. Small Molecule Organic Semiconductors on the Move: Promises for Future Solar Energy Technology. *Angew. Chem., Int. Ed.* **2012**, *51*, 2020–2067.
- (6) Walker, B.; Kim, C.; Nguyen, T.-Q. Small Molecule Solution-Processed Bulk Heterojunction Solar Cells. *Chem. Mater.* **2011**, *23*, 470–482.
- (7) Søndergaard, R.; Hösel, M.; Angmo, D.; Larsen-Olsen, T. T.; Krebs, F. C. Roll-to-Roll Fabrication of Polymer Solar Cells. *Mater. Today* **2012**, *15*, 36–49.
- (8) Boudreault, P.-L. T.; Najari, A.; Leclerc, M. Processable Low-Bandgap Polymers for Photovoltaic Applications. *Chem. Mater.* **2011**, *23*, 456–469.
- (9) Zhou, J.; Wan, X.; Liu, Y.; Zuo, Y.; Li, Z.; He, G.; Long, G.; Ni, W.; Li, C.; Su, X.; Chen, Y. Small Molecules Based on Benzo[1,2-b:4,5-b']dithiophene Unit for High-Performance Solution-Processed Organic Solar Cells. *J. Am. Chem. Soc.* **2012**, *134*, 16345–16351.
- (10) van der Poll, T. S.; Love, J. A.; Nguyen, T.-Q.; Bazan, G. C. Non-Basic High-Performance Molecules for Solution-Processed Organic Solar Cells. *Adv. Mater.* **2012**, *24*, 3646–3649.
- (11) Kyaw, A. K. K.; Wang, D. H.; Gupta, V.; Zhang, J.; Chand, S.; Bazan, G. C.; Heeger, A. J. Efficient Solution-Processed Small-Molecule Solar Cells with Inverted Structure. *Adv. Mater.* **2013**, *25*, 2397–2402.
- (12) Lin, Y.; Li, Y.; Zhan, X. Small Molecule Semiconductors for High-Efficiency Organic Photovoltaics. *Chem. Soc. Rev.* **2012**, *41*, 4245–4272.

- (13) Sun, Y.; Welch, G. C.; Leong, W. L.; Takacs, C. J.; Bazan, G. C.; Heeger, A. J. Solution-Processed Small-Molecule Solar Cells with 6.7% Efficiency. *Nat. Mater.* **2012**, *11*, 44–48.
- (14) Love, J. A.; Proctor, C. M.; Liu, J.; Takacs, C. J.; Sharek, A.; van der Poll, T. S.; Heeger, A. J.; Bazan, G. C.; Nguyen, T.-Q. Film Morphology of High Efficiency Solution-Processed Small-Molecule Solar Cells. *Adv. Funct. Mater.* **2013**, *23*, 5019–5026.
- (15) Venkataraman, D.; Yurt, S.; Venkatraman, B. H.; Gavvalapalli, N. Role of Molecular Architecture in Organic Photovoltaic Cells. *J. Phys. Chem. Lett.* **2013**, *1*, 947–958.
- (16) Takacs, C. J.; Sun, Y.; Welch, G. C.; Perez, L. A.; Liu, X.; Wen, W.; Bazan, G. C.; Heeger, A. J. Solar Cell Efficiency, Self-Assembly, and Dipole–Dipole Interactions of Isomeric Narrow-Band-Gap Molecules. *J. Am. Chem. Soc.* **2012**, *134*, 16597–16606.
- (17) Giridharagopal, R.; Ginger, D. S. Characterizing Morphology in Bulk Heterojunction Organic Photovoltaic Systems. *J. Phys. Chem. Lett.* **2010**, *1*, 1160–1169.
- (18) Zhugayevych, A.; Postupna, O.; Bakus, I.; Ronald, C.; Welch, G. C.; Bazan, G. C.; Tretiak, S. Ab Initio Study of a Molecular Crystal for Photovoltaics: Light Absorption, Exciton and Charge Carrier Transport. *J. Phys. Chem. C* **2013**, *117*, 4920–4930.
- (19) Peet, J.; Senatore, M. L.; Heeger, A. J.; Bazan, G. C. The Role of Processing in the Fabrication and Optimization of Plastic Solar Cells. *Adv. Mater.* **2009**, *21*, 1521–1527.
- (20) Pivrikas, A.; Neugebauer, H.; Sariciftci, N. S. Influence of Processing Additives to Nano-Morphology and Efficiency of Bulk-Heterojunction Solar Cells: A Comparative Review. *Sol. Energy* **2011**, *85*, 1226–1237.
- (21) Zhou, H.; Yang, L.; You, W. Rational Design of High Performance Conjugated Polymers for Organic Solar Cells. *Macromolecules* **2012**, *45*, 607–632.
- (22) Beaujuge, P. M.; Fréchet, J. M. J. Molecular Design and Ordering Effects in π -Functional Materials for Transistor and Solar Cell Applications. *J. Am. Chem. Soc.* **2011**, *133*, 20009–20029.
- (23) Facchetti, A. π -Conjugated Polymers for Organic Electronics and Photovoltaic Cell Applications. *Chem. Mater.* **2011**, *23*, 733–758.
- (24) Henson, Z. B.; Mullen, K.; Bazan, G. C. Design Strategies for Organic Semiconductors beyond the Molecular Formula. *Nat. Chem.* **2012**, *4*, 699–704.
- (25) Duan, C.; Huang, F.; Cao, Y. Recent Development of Push–Pull Conjugated Polymers for Bulk-Heterojunction Photovoltaics: Rational Design and Fine Tailoring of Molecular Structures. *J. Mater. Chem.* **2012**, *22*, 10416–10434.
- (26) Cheng, Y.-J.; Yang, S.-H.; Hsu, C.-S. Synthesis of Conjugated Polymers for Organic Solar Cell Applications. *Chem. Rev.* **2013**, *109*, 5868–5923.
- (27) Brédas, J.-L.; Norton, J. E.; Cornil, J.; Coropceanu, V. Molecular Understanding of Organic Solar Cells: The Challenges. *Acc. Chem. Res.* **2009**, *42*, 1691–1699.
- (28) Hachmann, J.; Olivares-Amaya, R.; Atahan-Evrénk, S.; Amador-Bedolla, C.; Sánchez-Carrera, R. S.; Gold-Parker, A.; Vogt, L.; Brockway, A. M.; Aspuru-Guzik, A. n. The Harvard Clean Energy Project: Large-Scale Computational Screening and Design of Organic Photovoltaics on the World Community Grid. *J. Phys. Chem. Lett.* **2011**, *2*, 2241–2251.
- (29) Pandey, L.; Risko, C.; Norton, J. E.; Brédas, J.-L. Donor–Acceptor Copolymers of Relevance for Organic Photovoltaics: A Theoretical Investigation of the Impact of Chemical Structure Modifications on the Electronic and Optical Properties. *Macromolecules* **2012**, *45*, 6405–6414.
- (30) Welch, G. C.; Bakus, I.; Ronald, C.; Teat, S. J.; Bazan, G. C. Impact of Regiochemistry and Isoelectronic Bridgehead Substitution on the Molecular Shape and Bulk Organization of Narrow Bandgap Chromophores. *J. Am. Chem. Soc.* **2013**, *135*, 2298–2305.
- (31) Bloking, J. T.; Han, X.; Higgs, A. T.; Kastrop, J. P.; Pandey, L.; Norton, J. E.; Risko, C.; Chen, C. E.; Brédas, J.-L.; McGehee, M. D.; Sellinger, A. Solution-Processed Organic Solar Cells with Power Conversion Efficiencies of 2.5% Using Benzothiadiazole/Imide-Based Acceptors. *Chem. Mater.* **2011**, *23*, 5484–5490.
- (32) Braunecker, W. A.; Oosterhout, S. D.; Owczarczyk, Z. R.; Larsen, R. E.; Larson, B. W.; Ginley, D. S.; Boltalina, O. V.; Strauss, S. H.; Kopidakis, N.; Olson, D. C. Ethynylene-Linked Donor–Acceptor Alternating Copolymers. *Macromolecules* **2013**, *46*, 3367–3375.
- (33) Huang, H.; Chen, Z.; Ortiz, R. P.; Newman, C.; Usta, H.; Lou, S.; Youn, J.; Noh, Y.-Y.; Baeg, K.-J.; Chen, L. X.; et al. Combining Electron-Neutral Building Blocks with Intramolecular “Conformational Locks” Affords Stable, High-Mobility p- and n-Channel Polymer Semiconductors. *J. Am. Chem. Soc.* **2012**, *134*, 10966–10973.
- (34) Hergué, N. m.; Mallet, C.; Savitha, G.; Allain, M.; Frère, P.; Roncali, J. Synthesis of 3-Alkoxy-4-cyanothiophenes as New Building Blocks for Donor–Acceptor Conjugated Systems. *Org. Lett.* **2011**, *13*, 1762–1765.
- (35) Guo, X.; Quinn, J.; Chen, Z.; Usta, H.; Zheng, Y.; Xia, Y.; Hennek, J. W.; Ortiz, R. P.; Marks, T. J.; Facchetti, A. Dialkoxybithiazole: A New Building Block for Head-to-Head Polymer Semiconductors. *J. Am. Chem. Soc.* **2013**, *135*, 1986–1996.
- (36) Ortiz, P. R.; Herrera, H.; Mancheño, M. J.; Seoane, C.; Segura, J. L.; Burrezo, P. M.; Casado, J.; López Navarrete, J. T.; Facchetti, A.; Marks, T. J. Molecular and Electronic-Structure Basis of the Ambipolar Behavior of Naphthalimide-Terthiophene Derivatives: Implementation in Organic Field-Effect Transistors. *Chem.—Eur. J.* **2013**, *19*, 12458–12467.
- (37) Ortiz, R. P.; Casado, J.; Hernández, V.; Navarrete, J. T. L.; Letizia, J. A.; Ratner, M. A.; Facchetti, A.; Marks, T. J. Thiophene-Diazine Molecular Semiconductors: Synthesis, Structural, Electrochemical, Optical, and Electronic Structural Properties; Implementation in Organic Field-Effect Transistors. *Chem.—Eur. J.* **2009**, *15*, 5023–5039.
- (38) Tian, Y.-H.; Kertesz, M. Low-Bandgap Pyrazine Polymers: Ladder-Type Connectivity by Intramolecular S···N(sp^2) Interactions and Hydrogen Bonds. *Macromolecules* **2009**, *42*, 2309.
- (39) Özen, A. S.; Atilgan, C.; Sonmez, G. Noncovalent Intramolecular Interactions in the Monomers and Oligomers of the Acceptor and Donor Type of Low Band Gap Conducting Polymers. *J. Phys. Chem. C* **2007**, *111*, 16362–16371.
- (40) Jackson, N. E.; Savoie, B. M.; Kohlstedt, K. L.; Olvera de la Cruz, M.; Schatz, G. C.; Chen, L. X.; Ratner, M. A. Controlling Conformations of Conjugated Polymers and Small Molecules: The Role of Nonbonding Interactions. *J. Am. Chem. Soc.* **2013**, *135*, 10475–10483.
- (41) Henson, Z. B.; Welch, G. C.; van der Poll, T.; Bazan, G. C. Pyridalthiadiazole-Based Narrow Band Gap Chromophores. *J. Am. Chem. Soc.* **2012**, *134*, 3766–3779.
- (42) Welch, G. C.; Perez, L. A.; Hoven, C. V.; Zhang, Y.; Dang, X.-D.; Sharek, A.; Toney, M. F.; Kramer, E. J.; Nguyen, T.-Q.; Bazan, G. C. A Modular Molecular Framework for Utility in Small-Molecule Solution-Processed Organic Photovoltaic Devices. *J. Mater. Chem.* **2011**, *21*, 12700–12709.
- (43) Garcia, A.; Welch, G. C.; Ratcliff, E. L.; Ginley, D. S.; Bazan, G. C.; Olson, D. C. Improvement of Interfacial Contacts for New Small-Molecule Bulk-Heterojunction Organic Photovoltaics. *Adv. Mater.* **2012**, *24*, 5368–5373.
- (44) Weinhold, F.; Landis, C. R. *Discovering Chemistry with Natural Bond Orbitals*; Wiley: New York, 2012.
- (45) Zhugayevych, A.; Lubchenko, V. Electronic Structure and the Glass Transition in Pnictide and Chalcogenide Semiconductor Alloys. I. The Formation of the pp σ -Network. *J. Chem. Phys.* **2010**, *133*, 234503.
- (46) Levine, I. N. *Physical Chemistry*; McGraw-Hill: New York, 2008.
- (47) Raos, G.; Famulari, A.; Marcon, V. Computational Reinvestigation of the Bithiophene Torsion Potential. *Chem. Phys. Lett.* **2003**, *379*, 364–372.
- (48) Riley, K. E.; Platts, J. A.; Řezáč, J.; Hobza, P.; Hill, J. G. Assessment of the Performance of MP2 and MP2 Variants for the Treatment of Noncovalent Interactions. *J. Phys. Chem. A* **2012**, *116*, 4159–4169.
- (49) Dahlgren, M. K.; Schyman, P.; Tirado-Rives, J.; Jorgensen, W. L. Characterization of Biaryl Torsional Energetics and its Treatment in

OPLS All-Atom Force Fields. *J. Chem. Inf. Model.* **2013**, *53*, 1191–1199.

(50) Choi, C. H.; Kertesz, M.; Karpfen, A. Limitations of Current Density Functional Theories for the Description of Partial π -Bond Breaking. *Chem. Phys. Lett.* **1997**, *276*, 266–268.

(51) Wang, Z.-X.; Duan, Y. Solvation Effects on Alanine Dipeptide: A MP2/cc-pVTZ//MP2/6-31G** Study of (Φ , Ψ) Energy Maps and Conformers in the Gas Phase, Ether, and Water. *J. Comput. Chem.* **2004**, *25*, 1699–1716.

(52) Yanai, T.; Tew, D. P.; Handy, N. C. A New Hybrid Exchange–Correlation Functional Using the Coulomb-Attenuating Method (CAM-B3LYP). *Chem. Phys. Lett.* **2004**, *393*, 51–57.

(53) Becke, A. D. Density Functional Thermochemistry. III. The Role of Exact Exchange. *J. Chem. Phys.* **1993**, *98*, 5648–5652.

(54) Takano, Y.; Houk, K. N. Benchmarking the Conductor-like Polarizable Continuum Model (CPCM) for Aqueous Solvation Free Energies of Neutral and Ionic Organic Molecules. *J. Chem. Theory Comput.* **2005**, *1*, 70–77.

(55) Sheldrick, G. M. A Short History of SHELX. *Acta Crystallogr. Sect. A* **2007**, *64*, 112–122.

Supporting Information for
A Combined Experimental and Theoretical Study of Conformational
Preferences of Molecular Semiconductors

Jessica E. Coughlin,^{†,§} Andriy Zhugayevych,[§] Ronald C. Bakus II,[†] Thomas S. van der Poll,[†] Gregory C. Welch,[†] Simon J. Teat,[‡] Guillermo C. Bazan,[†] and Sergei Tretiak[§]

[†] *Center for Polymers and Organic Solids, Departments of Chemistry & Biochemistry and Materials, University of California, Santa Barbara, California 93106, USA*

[§] *Theoretical Division, Center for Nonlinear Studies and Center for Integrated Nanotechnologies, Los Alamos National Laboratory, Los Alamos, NM 87545, USA*

[‡] *Advanced Light Source, Lawrence Berkeley National Laboratory, 1 Cyclotron Road, Mail Stop 15-317, Berkeley, California 94720, United States*

Contents

Donor-Acceptor (D-A) Molecule Optimization and Analysis.....	2
Calculated structural and electronic properties of molecules 1-8	5
Details on NBO analysis	13
Synthetic Procedures.....	17
Crystallographic Information.....	19

Donor-Acceptor (D-A) Molecule Optimization and Analysis

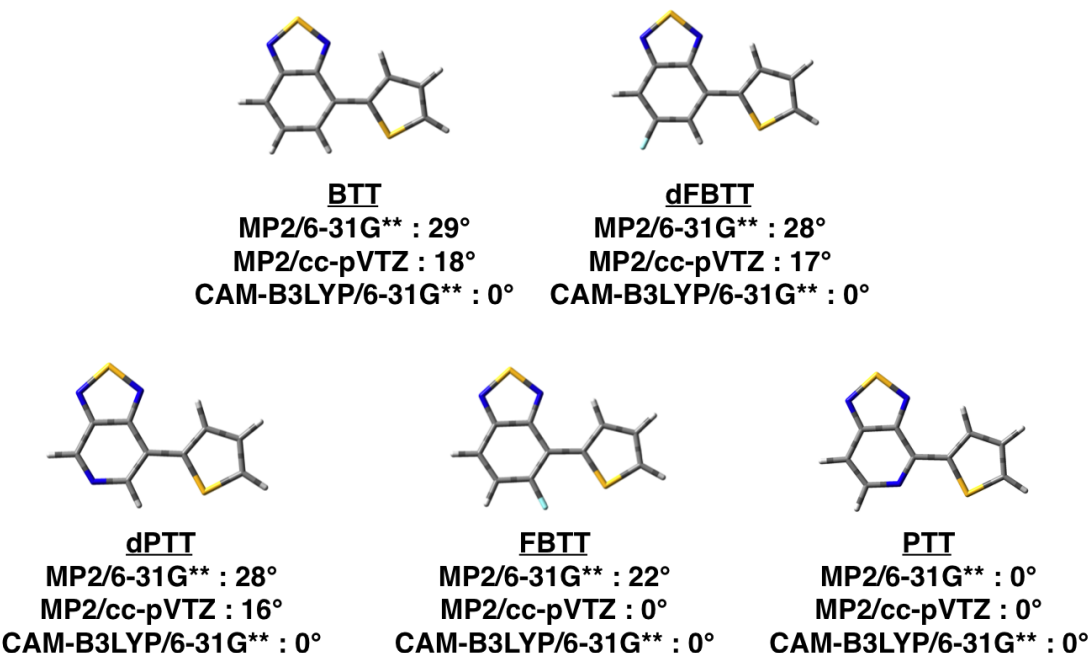


Figure S1. Optimized donor-acceptor structures from different functionals and basis sets.

Table S1. Total molecule energies of small molecules for both DFT and MP2 optimized and inverted dihedral geometries.

Molecule	Total Molecular Energies (Hartrees)			
	DFT		MP2	
	Optimized	Inverted	Optimized	Inverted
BTT	-1290.256341	-1290.255028	-1286.047961	-1286.042573
FBTT	-1389.469762	-1389.468557	-1384.8922	-1384.890274
FBOT	-1066.41719	-1066.414782	-1062.156351	-1062.153317
PTT	-1306.295307	-1306.292817	-1302.039156	-1302.032425
dFBTT	-1389.469884	-1389.468661	-1384.895759	-1384.890688
dFBOT	-1066.417134	-1066.41469	-1062.159346	-1062.154228
dPTT	-1306.288452	-1306.287213	-1302.031707	-1302.02742

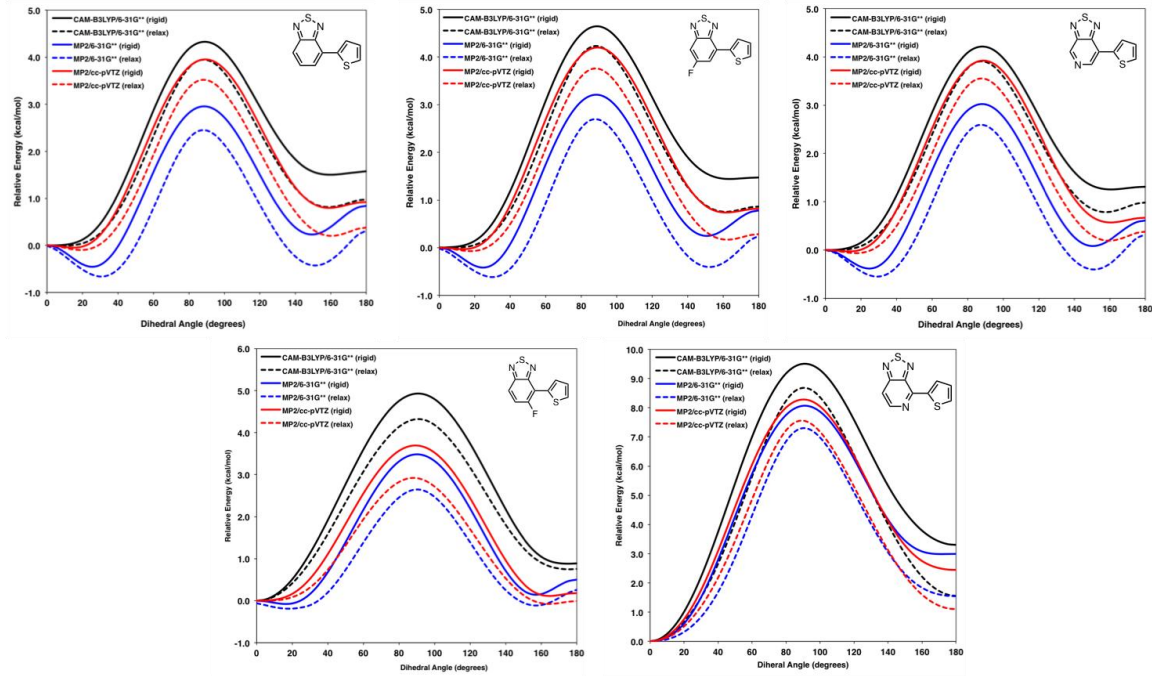


Figure S2. Rotational barriers for donor-acceptor molecules using different functional and basis sets.

Table S2. Second order perturbative stabilization energies for the optimized geometry structures calculated from the NBO5.9 software.

Second Order Perturbation Interaction Energies		
Molecule	Interaction	E(2) kcal/mol
FBTT	F (lp1); σ* S-C	0.82
	F (lp2); σ* S-C	2.35
	N17 (lp1); σ* C-H	3.10
dFBTT	S (lp1); σ* C-H	0.71
	N16 (lp1); σ* C-H	2.69
FBOT	F (lp1); σ* S-C	0.70
	F (lp2); σ* S-C	2.01
	N17 (lp1); σ* C-H	2.63
dFBOT	S (lp1); σ* C-H	0.54
	N16 (lp1); σ* C-H	2.36
BTT	S (lp1); σ* C-H	0.77
	N17 (lp1); σ* C-H	2.49
PTT	N (lp1); σ* S-C	0.53
	N (lp1); σ* S-C	1.52
	N17 (lp1); σ* C-H	1.95
dPTT	S (lp1); σ* C-H	0.72
	N16 (lp1); σ* C-H	2.38

Calculated structural and electronic properties of molecules 1-8

The optimized geometries are provided in the xyzfiles.zip folder.

Table S3. Total molecular energies for full molecules 1-8 for optimized, inverted wing, and inverted end geometries using CAM-B3LYP/6-31G**.

Total Molecular Energies (Hartrees)			
Molecule	Optimized	Inverted D-A bond	Inverted A-D' bond
1	-4082.951611	-4082.94703	-4082.948864
2	-4082.950373	-4082.947797	-4082.945868
3	-4050.872732	-4050.870162	-4050.870094
4	-3744.091099	-3744.088581	-3744.089364
5	-3744.10821	-3744.103558	-3744.094926
6	-5431.33957	-5431.337856	-5431.337241
7	-5431.339451	-5431.337364	-5431.337667
8	-5264.991354	-5264.98672	-5264.988502

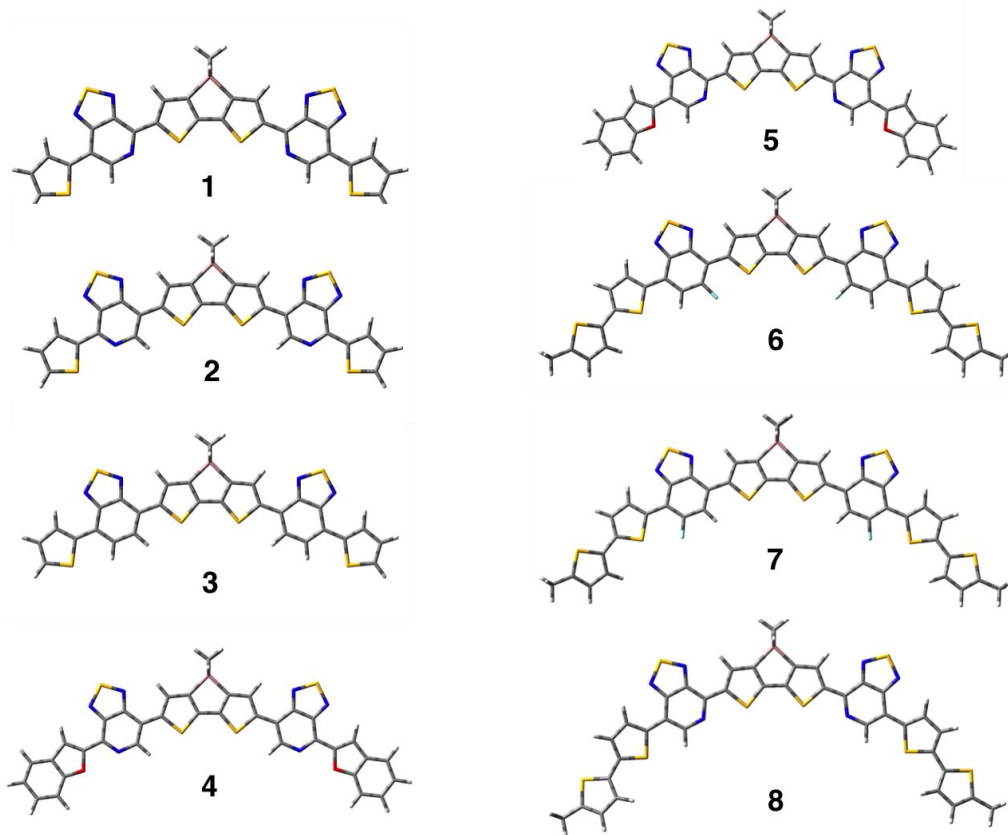
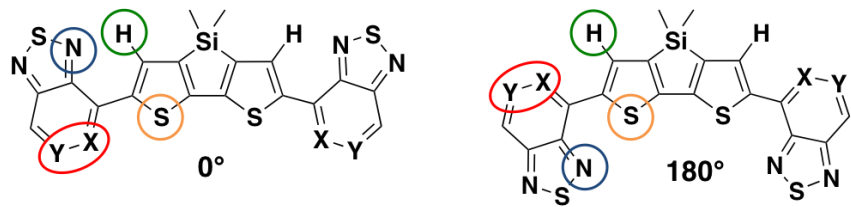


Figure S3. Calculated optimized structures of molecules 1-8.

Table S4. Differential energies entering Figure 11 (kcal/mol). All geometries are fully relaxed in C₂ symmetry. Prime means hydrogens in place of methyl groups, star means additional thiophene terminal unit. Calculations in vaccum are marked by “vac”, those in chloroform are marked by “clf”.

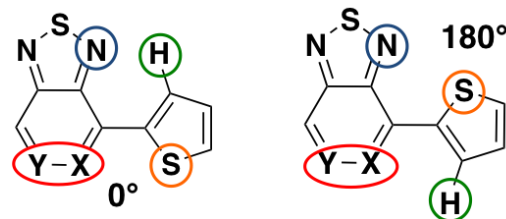
	DTS-A vac	DTS-A clf	A-D' vac	A-D' clf
1	2.88	2.93	1.72	0.84
2	1.37	0.44	2.83	2.83
3	1.61	0.53	1.66	0.44
4	1.36	0.66	1.09	1.67
5	2.91	2.97	7.57	5.88
6	1.08	0.76	1.42	0.41
7	1.27	0.19	1.12	0.81
8=1*	2.91	2.96	1.63	0.70
8'=1'*	2.99	2.96	1.50	0.57
2'*	1.22	0.30	2.95	2.94
6'	1.06	0.76	1.26	0.25
7'	0.96	-0.02	1.14	0.83

Table S5. Natural atomic charges for molecules 1-8 generated from the natural population analysis.



Natural Atomic Charges (A-D-A)							
Molecule	Dihedral Angle	Thiadiazole Nitrogen	Hydrogen	Sulfur	Fluorine	Pyridal Nitrogen	Carbon
1	0°	-0.629	0.273	0.538	-	-0.458	-
	180°	-0.626	0.272	0.532	-	-0.455	-
2	0°	-0.647	0.275	0.477	-	-0.454	0.023
	180°	-0.643	0.247	0.531	-	-0.455	0.025
3	0°	-0.648	0.277	0.470	-	-	-0.212
	180°	-0.644	0.244	0.538	-	-	-0.161
4	0°	-0.646	0.274	0.480	-	-0.422	0.018
	180°	-0.642	0.248	0.532	-	-0.424	0.026
5	0°	-0.628	0.273	0.541	-	-0.462	-
	180°	-0.625	0.272	0.533	-	-0.458	-
6	0°	-0.651	0.275	0.507	-0.330	-	-
	180°	-0.647	0.263	0.529	-0.335	-	-
7	0°	-0.644	0.278	0.476	-0.329	-	-0.274
	180°	-0.640	0.245	0.541	-0.331	-	-0.267
8	0°	-0.630	0.273	0.538	-	-0.458	-
	180°	-0.627	0.272	0.531	-	-0.454	-

Table S6. Natural atomic charges for molecules 1-8 generated from the natural population analysis.



Natural Atomic Charges (A-D')							
Molecule	Dihedral Angle	Nitrogen	Hydrogen (Hydrogen on A)	Sulfur (or Oxygen*)	Fluorine	Pyridal Nitrogen	Carbon
1	0°	-0.646	0.274	0.451	-	-0.458	0.025
	180°	-0.642	0.247	0.503	-	-0.458	0.035
2	0°	-0.627	0.272	0.508	-	-0.454	-
	180°	-0.625	0.271	0.503	-	-0.450	-
3	0°	-0.647	0.276	0.444	-	-	-0.209
	180°	-0.643	0.244	0.509	-	-	-0.201
4*	0°	-0.629	0.275 (0.255)	-0.455	-	-0.422	0.039
	180°	-0.598	0.272 (0.237)	-0.452	-	-0.441	0.042
5*	0°	-0.643	0.275	-0.473	-	-0.462	-
	180°	-0.631	0.254	-0.451	-	-0.464	-
6	0°	-0.641	0.278	0.456	-0.330	-	-0.273
	180°	-0.639	0.247	0.519	-0.331	-	-0.265
7	0°	-0.649	0.276	0.487	-0.329	-	-
	180°	-0.646	0.264	0.509	-0.333	-	-
8	0°	-0.645	0.275	0.457	-	-0.458	0.025
	180°	-0.642	0.249	0.510	-	-0.459	0.035

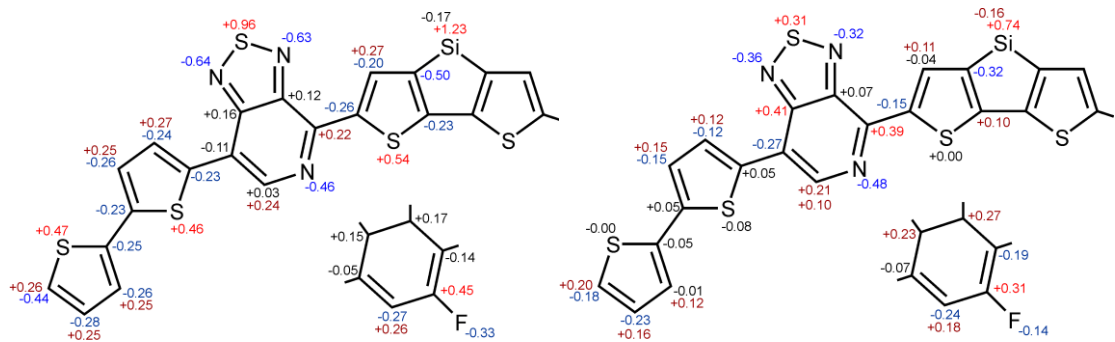
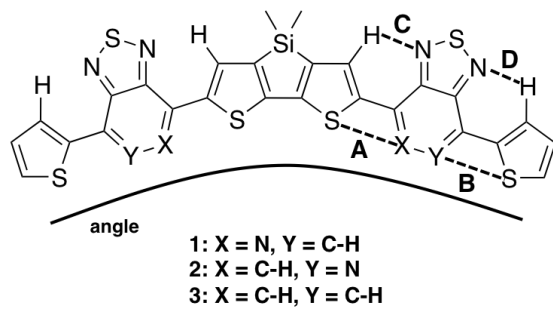


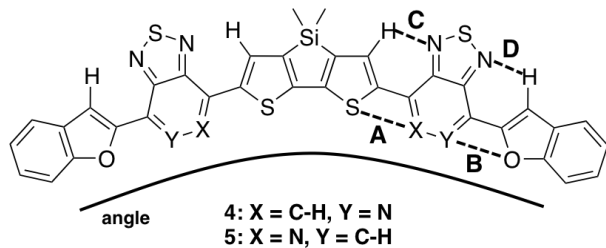
Figure S4. NBO (left) and vdw (right) charges for molecules **6** and **8**.

Table S7. Intramolecular atom distances and molecule angles for molecules **1-3**. Distances averaged from both sides of the molecule.



Atomic Distances [Sum of van der Waals radii] (Å)			
Distance	1	2	3
A	2.91 [3.35]	3.12 [3.5]	3.10 [3.5]
B	3.12 [3.5]	2.92 [3.35]	3.11 [3.5]
C	2.39 [2.75]	2.33 [2.75]	2.30 [2.75]
D	2.34 [2.75]	2.40 [2.75]	2.31 [2.75]
Molecule Angle	115.2°	117.8°	121.2°

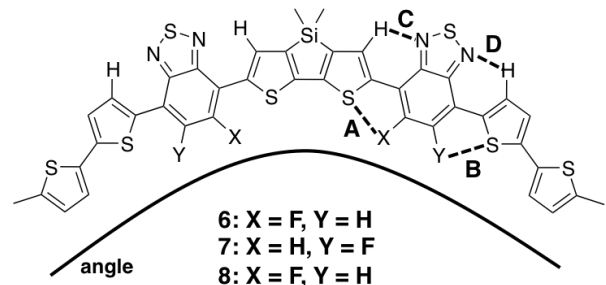
Table S8. Intramolecular atom distances and molecule angles for molecules **4** and **5**. Distances averaged from both sides of the molecule.



Atom Distances [Sum of van der Waals radii] (Å)

Distance	4	5
A	3.12 [3.5]	2.91 [3.35]
B	2.69 [3.02]	2.78 [3.22]
C	2.33 [2.75]	2.39 [2.75]
D	2.46 [2.75]	2.51 [2.75]
Molecular Angle	117.9°	114.1°

Table S9. Intramolecular atom distances and molecule angles for molecules **6-8**. Distances averaged from both sides of the molecule. *Molecule **8** distance A was measured from the pyridyl nitrogen to the DTS sulfur.



Atom Distances [Sum of van der Waals radii] (Å)

Distance	6	7	8
A	2.70 [3.2]	2.67 [3.05]	2.91* [3.35]
B	2.69 [3.05]	2.70 [3.2]	2.68 [3.0]
C	2.26 [2.75]	2.30 [2.75]	2.39 [2.75]
D	2.33 [2.75]	2.27 [2.75]	2.35 [2.75]
Molecular Angle	123.4°	121.6°	115.2°

Table S10. Second Order Perturbation Energies for inverted bond 1 and 1'.

Second Order Perturbation Interaction Energies		
Molecule	Interaction (donor;acceptor)	E(2) kcal/mol
1	Pyridal N (lp); σ^* SDT C-H	0.57
	Thiadiazole N (lp); σ^* SDT S-C	2.05
	Thiadiazole N (lp); σ^* Thiophene C-H	2.33
2	Pyridal N (lp); σ^* Thiophene S-C	2.01
	Thiadiazole N (lp); σ^* SDT S-C	2.26
	Thiadiazole N (lp); σ^* Thiophene C-H	1.86
3	Thiadiazole N (lp1); σ^* SDT S-C	2.71
	Thiadiazole N (lp1); σ^* Thiophene C-H	2.60
	Thiophene S; σ^* BT C-H	0.80
4	Thiadiazole N (lp); σ^* Bz C-H	1.39
	Thiadiazole N (lp); σ^* SDT S-C	2.25
5	Thiadiazole N (lp); σ^* SDT S-C	2.03
	Thiadiazole N (lp); σ^* Bz C-H	1.19
	Pyridal N (lp); σ^* SDT C-H	0.58
	Bz O (lp1); σ^* PT C-H	0.54
6	F (lp); σ^* SDT C-H	2.56
	Thiadiazole N (lp); σ^* SDT S-C	2.99
	Thiadiazole N (lp); σ^* Thiophene C-H	2.49
	Thiophene S (lp); σ^* FBT C-H	0.65
7	F (lp); σ^* Thiophene S-C	3.33
	Thiadiazole N (lp); σ^* SDT S-C	2.68
	Thiadiazole N (lp); σ^* Thiophene C-H	3.01
8	Thiadiazole N (lp); σ^* SDT S-C	2.05
	Thiadiazole N (lp); σ^* Thiophene C-H	2.22
	Pyridal N (lp); σ^* SDT C-H	0.57

Table S11. 2nd Order Perturbation Energies for inverted bond between the acceptor unit and end donor unit.

Second Order Perturbation Interaction Energies		
Molecule	Interaction (donor;acceptor)	E(2) kcal/mol
1	Pyridal N (lp); σ* SDT S-C	2.24
	Thiadiazole N (lp); σ* SDT C-H	2.00
	Thiadiazole N (lp); σ* Thiophene S-C	2.03
2	Pyridal N (lp); σ* Thiophene S-C	2.24
	Thiadiazole N (lp); σ* Thiophene S-C	1.83
	SDT S; σ* PT C-H	0.72
3	Thiadiazole N (lp1); σ* SDT C-H	2.80
	Thiadiazole N (lp1); σ* Thiophene S-C	2.44
	SDT S; σ* BT C-H	0.79
4	Thiadiazole N (lp); σ* SDT C-H	2.62
	SDT S (lp); σ* PT C-H	0.73
5	Thiadiazole N (lp); σ* SDT S-C	2.29
	Thiadiazole N (lp); σ* SDT C-H	2.09
6	F (lp); σ* SDT S-C	3.42
	Thiadiazole N (lp); σ* SDT C-H	3.22
	Thiadiazole N (lp); σ* Thiophene S-C	2.61
7	F (lp); σ* Thiophene C-H	2.37
	Thiadiazole N (lp); σ* SDT C-H	2.76
	Thiadiazole N (lp); σ* Thiophene S-C	2.91
	SDT S (lp); σ* FBT C-H	1.23
8	Pyridal N (lp); σ* Thiophene S-C	2.23
	Thiadiazole N (lp); σ* SDT C-H	2.00
	Thiadiazole N (lp); σ* Thiophene S-C	2.20

Details on NBO analysis

Raw data for the NBO analysis are collected in nbo.zip file including geometry, output of the Gaussian program, and postprocessing of the standard NBO analysis for each rotamer.

List of molecules used for Figure 3a:

BO+BF, BO+BTh, BO+F, BO+T, BO+TT, BT+BF, BT+BTh, BT+F, BT+T, BT+TT, FBO+T, FBT+T, FP+T, P+BF, P+BTh, P+F, P+T, P+TT, PBO+T, PBT+T, PO+T, PP+T, PT+BF, PT+BTh, PT+F, PT+T, PT+TT, T+T, dFBT+T, dPT+BF, dPT+T

List of molecules used for Figure 3b:

BO+BF, BO+BTh, BO+F, BO+T, BO+TT, BP+BF, BP+BTh, BP+F, BP+T, BP+TT, BT+BF, BT+BTh, BT+F, BT+T, BT+TT, FB+BF, FB+BTh, FB+F, FB+T, FB+TT, FBO+T, FBT+T, FFB+T, FP+T, P+BF, P+BTh, P+F, P+T, P+TT, PBO+T, PBT+T, PFB+T, PO+T, PP+T, PT+BF, PT+BTh, PT+F, PT+T, PT+TT, T+T, dFBT+T, dPT+BF, dPT+T

Notations:

- BF – benzofuran
- BO – 2,1,3-benzoxadiazole (benzofurazan)
- BP – benzopyrazine (quinoxaline)
- BT – benzo[1,2,5]thiadiazole
- BTh – benzothiophene
- F – furan
- FB – fluorobenzene
- FBO – fused FB and BO
- FBT – 5-fluorobenzo[c][1,2,5]thiadiazole
- FFB – 1,2-difluorobenzene
- FP – 3-fluoropyridine
- P – pyridine
- PBO – fused BP and BO
- PBT – fused BP and BT
- PFB – fused BP and FB
- PO – [1,2,5]oxadiazolo[3,4-c]pyridine
- PP – pyrazino[2,3-d]pyridazine
- PT – [1,2,5]thiadiazolo[3,4-c]pyridine
- T – thiophene
- TBO – fused BT and BO
- TT – thienothiophene

Dielectric screening is taken into account by replacing the bare Coulomb interaction $1/r$ by $1/r - 1/\sqrt{r^2 + a^2}$ with $a=3 \text{ \AA}$.

Table S12. Full set of differential energies (in kcal/mol) for the dihedrals listed in Table 2. Notations: NBO = unit-wise NBO analysis, NBO' = atom-wise NBO analysis used in the main text, core/pi/sigma = near-bridge bonds orbital interactions involving core electrons, π -bonds, and σ -bonds respectively, cc1/cc2 = close-contact orbital interactions involving σ -bonds and lone pairs, solv = differential solvation energy in chloroform, ES' = sum of electrostatic interactions between close-contact atoms.

PT+T:					dPT+T:				
	DA	EX	ES	total		DA	EX	ES	total
exact				1.56	exact				0.79
NBO	4.4	0.9	0.6	5.9	NBO	6.5	-1.8	-1.7	3.1
NBO'	6.0	0.6	-1.7	4.9	NBO'	9.3	-3.7	-3.5	2.1
core	0.1	0.1	0.0	0.2	core	-3.2	2.7	0.0	-0.5
pi	3.2	0.8	0.0	4.0	pi	7.0	-1.2	0.0	5.8
sigma	1.4	-0.7	0.1	0.8	sigma	1.8	-1.4	0.0	0.4
cc1	0.2	0.7	-3.0	-2.1	cc1	2.2	-2.3	-2.2	-2.3
cc2	1.1	-0.3	1.2	2.0	cc2	1.5	-1.5	-1.3	-1.3
solv				0.03	solv				0.48
ES'				-2.5	ES'				5.5
PT+BF:					dPT+BF:				
	DA	EX	ES	total		DA	EX	ES	total
exact				0.65	exact				3.78
NBO	3.7	-1.2	1.6	4.1	NBO	6.8	-2.0	7.9	12.7
NBO'	4.3	-0.6	3.1	6.8	NBO'	10.7	-4.8	5.3	11.2
core	-0.1	0.1	0.0	0.1	core	-5.0	3.7	0.0	-1.2
pi	2.5	1.0	0.0	3.5	pi	10.1	-2.3	0.0	7.8
sigma	0.4	-0.2	-0.9	-0.7	sigma	2.4	-1.9	0.3	0.8
cc1	2.2	-2.1	3.9	4.0	cc1	2.5	-2.7	3.1	3.0
cc2	-0.7	0.6	0.1	0.0	cc2	0.6	-1.7	1.8	0.8
solv				-0.21	solv				0.90
ES'				-7.4	ES'				27.8
FBT+T:					dFBT+T:				
	DA	EX	ES	total		DA	EX	ES	total
exact				0.76	exact				0.75
NBO	2.6	0.9	-1.0	2.5	NBO	5.2	-0.8	-1.5	3.0
NBO'	3.8	0.7	-3.3	1.2	NBO'	7.6	-2.0	-2.8	2.8
core	0.1	-0.0	0.0	0.1	core	-2.0	1.7	0.0	-0.3
pi	2.4	0.5	0.0	2.9	pi	5.5	-0.4	0.0	5.1
sigma	0.1	-0.1	-0.0	0.0	sigma	1.2	-0.9	-0.0	0.3
cc1	0.7	0.8	-3.1	-1.6	cc1	1.6	-1.2	-2.8	-2.4
cc2	0.5	-0.5	-0.3	-0.3	cc2	1.2	-1.1	0.0	0.1
solv				0.21	solv				0.51
ES'				2.7	ES'				8.8

BT+T:					BP+T:				
	DA	EX	ES	total		DA	EX	ES	total
exact				0.82	exact				-0.30
NBO	5.4	-0.8	-1.5	3.1	NBO	-0.3	3.7	-2.0	1.4
NBO'	7.8	-2.8	-3.1	1.9	NBO'	-1.4	3.8	-2.6	-0.3
core	-2.4	1.9	0.0	-0.4	core	1.3	-1.4	0.0	-0.1
pi	5.8	-0.8	0.0	5.0	pi	-0.2	1.0	0.0	0.9
sigma	1.4	-1.1	0.0	0.3	sigma	-0.7	0.7	-0.1	-0.1
cc1	1.6	-1.5	-2.7	-2.6	cc1	-2.3	3.1	-2.2	-1.4
cc2	1.3	-1.3	-0.4	-0.5	cc2	0.4	0.4	-0.3	0.5
solv				0.53	solv				0.27
ES'				7.6	ES'				10.9

T+T:				
	DA	EX	ES	total
exact				0.64
NBO	2.7	0.1	0.9	3.6
NBO'	2.8	-0.7	2.7	4.9
core	-3.8	2.6	0.0	-1.3
pi	4.6	-1.4	0.0	3.3
sigma	1.8	-1.1	0.2	0.9
cc1	-0.0	-0.3	2.2	1.9
cc2	0.2	-0.5	0.3	0.1
solv				0.07
ES'				1.3

Table S13. Summary of Table S12.

	exact	NBO	NBO'	solv	ES'
PT+T (blue)	1.56	5.6	5.1	0.03	-2.5
dPT+T (red)	0.79	3.5	2.5	0.48	5.5
PT+BF (gray)	0.65	3.3	4.7	-0.21	-7.4
dPT+BF (light blue)	3.78	7.5	6.8	0.90	27.8
FBT+T (green)	0.76	2.6	1.4	0.21	2.7
dFBT+T (purple)	0.75	3.2	3.0	0.51	8.8
BT+T (orange)	0.82	3.4	2.1	0.53	7.6
BP+T	-0.30	1.4	-0.3	0.27	10.9
T+T	0.64	3.6	4.9	0.07	1.3

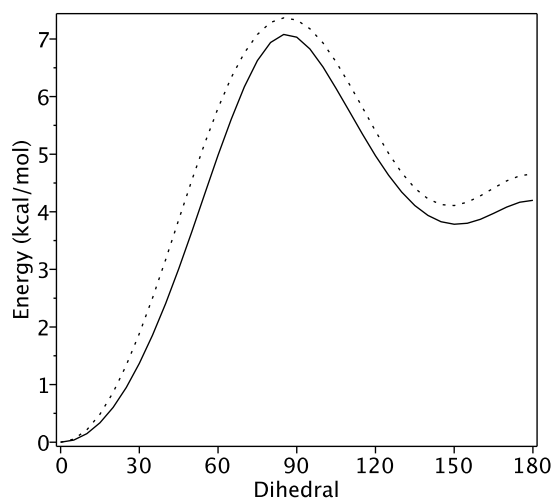


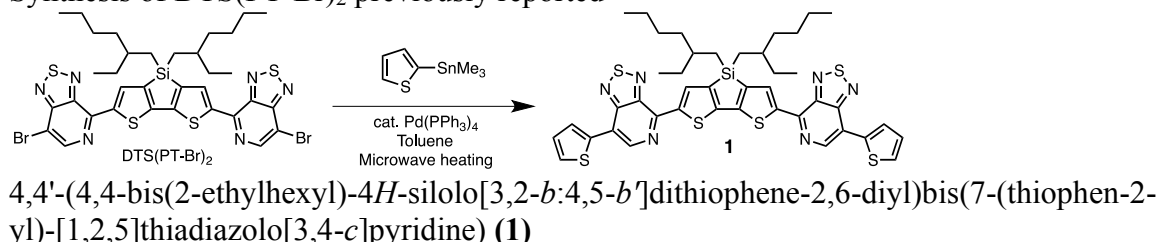
Figure S5. Potential energy scan using a finer grid for the dPT+BF fragment in vacuum. The dotted line represents the rigid scan and the solid line is the relaxed scan.

Synthetic Procedures

Molecules **2**, **4**, **5**, **6**, and **8** have been previously reported.

Molecule 1:

Synthesis of DTS(PT-Br)₂ previously reported³

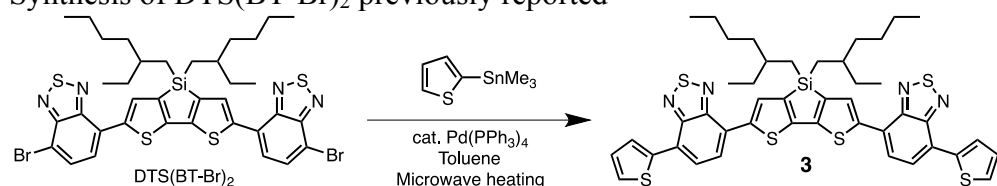


4,4'-(4,4-bis(2-ethylhexyl)-4H-silolo[3,2-b:4,5-b']dithiophene-2,6-diyl)bis(7-(thiophen-2-yl)-[1,2,5]thiadiazolo[3,4-c]pyridine) (**1**)

In a N₂ filled glove box a 10 mL glass tube was charged with DTS(PT-Br₂) (150 mg, 0.18 mmol), 2-(tributylstannylyl)thiophene (160 mg, 0.39 mmol), Pd(PPh₃)₄ (10 mg, 0.008 mmol) and toluene (3 mL), and sealed with a Teflon® cap. The reaction mixture was heated to 80 °C for 1 minute, 110 °C for 1 minute, and 140 °C for 45 minutes using a Biotage microwave reactor. Upon cooling, the reaction solution was eluted through a silica gel plug with chloroform and then the solvents were removed in vacuo. The solid was washed with hexanes (50 mL x 3) and then methanol (30 mL x 3), to give a purple shiny solid. Recovered yield: 98 mg (65%). ¹H NMR (CDCl₃): δ 8.85 (s, 2H, CH), 8.78 (t, 2H, CH), 8.11 (d, 2H, CH), 7.49 (d, 2H, CH), 7.24 (d, 2H, CH), 1.1-1.4 (broad m, 18H, CH₂), 0.7-0.8 (broad m, 12H, CH₃). ¹³C NMR (CDCl₃) 20 of 21 found: δ 154.9, 148.03, 147.48, 146.37, 141.07, 136.76, 135.39, 128.14, 127.62, 127.05, 119.83, 103.73, 36.06, 35.8, 29.02, 28.97, 23.03, 17.7, 14.22, 10.85. LRMS (FD) *m/z*, calculated (M⁺): 852.17, found: 852.11.

Molecule 3:

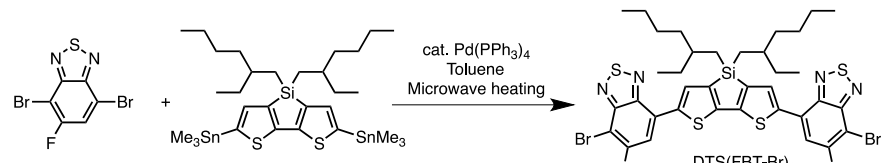
Synthesis of DTS(BT-Br)₂ previously reported⁴



7,7'-(4,4-bis(2-ethylhexyl)-4H-silolo[3,2-b:4,5-b']dithiophene-2,6-diyl)bis(4-(thiophen-2-yl)benzo[c][1,2,5]thiadiazole) (**3**)

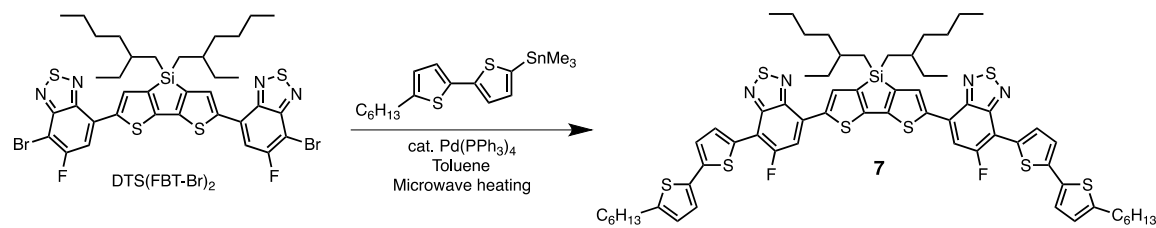
Synthesized using the same procedure as molecule 1. Recovered yield: 30 mg (75%). ¹H NMR (CDCl₃): δ 8.85 (s, 2H, CH), 8.78 (t, 2H, CH), 8.11 (d, 2H, CH), 7.49 (d, 2H, CH), 7.24 (d, 2H, CH), 1.1-1.4 (broad m, 18H, CH₂), 0.7-0.8 (broad m, 12H, CH₃). ¹³C NMR (CDCl₃) 22 of 22 found: δ 150.34, 144.80, 140.97, 140.95, 139.51, 130.72, 128.0, 127.31, 126.62, 126.33, 125.9, 125.28, 124.78, 36.04, 35.76, 28.99, 28.96, 23.05, 17.78, 14.21, 10.87. LRMS (FD) *m/z*, calculated (M⁺): 850, found: 850.

Molecule 7:



7,7'-(4,4-Bis(2-ethylhexyl)-4H-silolo[3,2-b:4,5-b']dithiophene-2,6-diyl)bis(6-fluoro-4-bromo-benzo[c][1,2,5]thiadiazole) (**DTS(FBT-Br)₂**)

In a N₂ filled glove box a 20 mL glass tube was charged with 4,7-Dibromo-5-fluorobenzo[c][1,2,5]thiadiazole (397 mg, 1.27 mmol), 5,5'-bis(trimethylstannyl)-3,3'-di-2-ethylhexylsilylene-2,2'-bithiophene (316 mg, 0.42 mmol), Pd(PPh₃)₄ (50 mg, 0.04 mmol) and toluene (15 mL), and sealed with a Teflon® cap. The reaction mixture was heated to 100 °C for 1 minute, 125 °C for 1 minute, 150 °C for 1 minute, and 165 °C for 30 minutes using a Biotage microwave reactor. Upon cooling, the material was then loaded onto silica and purified by flash chromatography using a hexanes/chloroform gradient. After fraction collection and solvent removal a purple solid was obtained. Recovered yield: 332 mg (90 %). **¹H NMR** (CDCl₃): δ □ 8.11 (t, 2H, CH), 7.65 (d, J = 10.2 Hz, 2H, CH), 1.43 (br m, 2H, CH₂), 1.25 (br m, 4H, CH₂), 1.18 (br m, 4H, CH₂), 1.11 (br m, 6H, CH₃), 1.00 (br m, 4H, CH₃), 0.73 (m, 12H, CH₃).



7,7'-(4,4-bis(2-ethylhexyl)-4H-silolo[3,2-b:4,5-b']dithiophene-2,6-diyl)bis(5-fluoro-4-(5'-hexyl-[2,2'-bithiophen]-5-yl)benzo[c][1,2,5] thiadiazole) (**7**)

In a N₂ filled glove box a 20 mL glass tube was charged with DTS(FBT-Br)₂ (100 mg, 0.11 mmol), 5'-hexyl-2,2'-bithiophene-5-trimethylstannane (94 mg, 0.23 mmol), Pd(PPh₃)₄ (30 mg, 0.024 mmol) and toluene (15 mL), and sealed with a Teflon® cap. The reaction mixture was heated to 100 °C for 1 minute, 125 °C for 1 minute, 150 °C for 1 minute, and 165 °C for 30 minutes using a Biotage microwave reactor. Upon cooling, the material was then loaded onto silica, washed with methanol and purified by flash chromatography using a hexanes/chloroform gradient *in duplicate*. After fraction collection and solvent removal a metallic purple solid was obtained. The solid was slurried in a 3:1 mixture of methanol and hexanes, sonicated for 1 hour and stirred overnight. The suspension was filtered, washed with acetone and dried in vacuo. The product was recovered as a metallic purple solid. Recovered yield: 79 mg (59 %). **¹H NMR** (CDCl₃): δ 8.20 (t, 2H, CH), 8.16 (d, J = 4.2 Hz, 2H, CH), 7.69 (d, J = 13.2 Hz, 2H, CH), 7.20 (d, J = 4.2 Hz, 2H, CH), 7.12 (d, J = 3.0 Hz, 2H, CH), 6.72 (d, J = 3.6 Hz, 2H, CH), 2.83 (t, J = 7.8 Hz, 4H, CH₂), 1.71 (m, 4H, CH₂), 1.56 (br m, 2H, CH₂), 1.40 (br m, 4H, CH₂), 1.33 (br m, 16H, CH₂), 1.24 (br m, 8H, CH₂), 1.12 (br m, 4H, CH₂), 0.90 (m, 6H, CH₃), 0.83 (br m, 12H, CH₃).

Crystallographic Information

The crystals for molecules **4¹**, **5¹**, and **8²** were previously reported.

Table S14. Crystal data and structure refinement for molecule **1**.

Identification code	rcb_g7p_nmr
Empirical formula	C42 H42 N6 S6 Si
Formula weight	851.27
Temperature	100(2) K
Wavelength	0.77490 Å
Crystal system	Triclinic
Space group	P-1
Unit cell dimensions	a = 10.4822(7) Å α = 67.272(2)° b = 13.6007(9) Å β = 88.286(2)° c = 16.4254(11) Å γ = 71.732(2)°
Volume	2039.9(2) Å ³
Z	2
Density (calculated)	1.386 Mg/m ³
Absorption coefficient	0.508 mm ⁻¹
F(000)	892
Crystal size	0.44 x 0.11 x 0.02 mm ³
Theta range for data collection	3.08 to 33.62°.
Index ranges	-14<=h<=14, -19<=k<=19, -23<=l<=23
Reflections collected	29769
Independent reflections	12218 [R(int) = 0.0555]
Completeness to theta = 33.62°	98.1 %
Absorption correction	Semi-empirical from equivalents
Max. and min. transmission	0.94 and 0.75
Refinement method	Full-matrix least-squares on F ²
Data / restraints / parameters	12218 / 784 / 657
Goodness-of-fit on F²	1.026
Final R indices [I>2sigma(I)]	R1 = 0.0663, wR2 = 0.1908
R indices (all data)	R1 = 0.0745, wR2 = 0.2004
Extinction coefficient	n/a
Largest diff. peak and hole	1.507 and -1.147 e.Å ⁻³

Table S15. Crystal data and structure refinement for molecule 2.

Identification code	g02252011_0m
Empirical formula	C42 H44 N6 S6 Si
Formula weight	853.28
Temperature	100(2) K
Wavelength	0.71073 Å
Crystal system	Monoclinic
Space group	P2(1)/n
Unit cell dimensions	a = 18.817(4) Å α = 90°
	b = 7.9805(17) Å β = 107.018(3)°
	c = 28.301(6) Å γ = 90°
Volume	4063.8(15) Å ³
Z	4
Density (calculated)	1.395 Mg/m ³
Absorption coefficient	0.407 mm ⁻¹
F(000)	1792
Crystal size	0.3 x 0.05 x 0.05 mm ³
Theta range for data collection	1.16 to 24.48°
Index ranges	-21<=h<=21, -9<=k<=8, -30<=l<=32
Reflections collected	19599
Independent reflections	6724 [R(int) = 0.0655]
Completeness to theta = 24.48°	99.6 %
Absorption correction	Multi scan
Max. and min. transmission	0.712 and 0.472
Refinement method	Full-matrix least-squares on F ²
Data / restraints / parameters	6724 / 7 / 500
Goodness-of-fit on F²	1.664
Final R indices [I>2sigma(I)]	R1 = 0.0841, wR2 = 0.1942
R indices (all data)	R1 = 0.1370, wR2 = 0.2111
Largest diff. peak and hole	0.833 and -0.448 e.Å ⁻³

Table S16. Crystal data and structure refinement for molecule **3**.

Identification code	g05042012_0m
Empirical formula	C44 H46 N4 S6 Si
Formula weight	851.30
Temperature	100(2) K
Wavelength	0.71073 Å
Crystal system	Monoclinic
Space group	P2(1)/c
Unit cell dimensions	a = 18.34(2) Å α = 90°
	b = 7.326(9) Å β = 103.18(5)°
	c = 31.80(5) Å γ = 90°
Volume	4159(10) Å ³
Z	4
Density (calculated)	1.360 Mg/m ³
Absorption coefficient	0.396 mm ⁻¹
F(000)	1792
Crystal size	0.03 x 0.01 x 0.01 mm ³
Theta range for data collection	1.32 to 26.31°
Index ranges	-22<=h<=21, -8<=k<=8, -16<=l<=39
Reflections collected	20461
Independent reflections	8069 [R(int) = 0.0750]
Completeness to theta = 26.31°	95.6 %
Absorption correction	Semi-empirical from equivalents
Max. and min. transmission	0.7454 and 0.6393
Refinement method	Full-matrix least-squares on F ²
Data / restraints / parameters	8069 / 62 / 466
Goodness-of-fit on F²	1.501
Final R indices [I>2sigma(I)]	R1 = 0.0961, wR2 = 0.2222
R indices (all data)	R1 = 0.1615, wR2 = 0.2436
Largest diff. peak and hole	1.267 and -0.751 e.Å ⁻³

Table S17. Crystal data and structure refinement for molecule **6**.

Identification code	t1
Empirical formula	C64 H8 F2 N4 S8 Si
Formula weight	1155.31
Temperature	150(2) K
Wavelength	0.77490 Å
Crystal system	Triclinic
Space group	P-1
Unit cell dimensions	a = 9.2539(11) Å α = 81.005(9)°
	b = 14.9631(19) Å β = 85.178(9)°
	c = 22.219(3) Å γ = 88.053(9)°
Volume	3027.3(6) Å ³
Z	2
Density (calculated)	1.267 Mg/m ³
Absorption coefficient	0.665 mm ⁻¹
F(000)	1160
Crystal size	0.15 x 0.03 x 0.00 mm ³
Theta range for data collection	1.50 to 21.23°
Index ranges	-8<=h<=8, -13<=k<=13, -20<=l<=20
Reflections collected	16271
Independent reflections	5158 [R(int) = 0.1010]
Completeness to theta = 21.23°	99.8 %
Max. and min. transmission	0.9980 and 0.9069
Refinement method	Full-matrix least-squares on F ²
Data / restraints / parameters	5158 / 92 / 629
Goodness-of-fit on F²	1.347
Final R indices [I>2sigma(I)]	R1 = 0.1361, wR2 = 0.3409
R indices (all data)	R1 = 0.1795, wR2 = 0.3698
Largest diff. peak and hole	1.347 and -0.605 e.Å ⁻³

Table S18. Crystal data and structure refinement for molecule 7.

Identification code	t2
Empirical formula	C64 H72 F2 N4 S8 Si
Formula weight	1219.82
Temperature	100(2) K
Wavelength	0.7749 Å
Crystal system	Triclinic
Space group	P -1
Unit cell dimensions	a = 8.808(3) Å α= 108.413(5)°
	b = 16.279(6) Å β= 100.019(6)°
	c = 22.976(9) Å γ = 95.249(5)°
Volume	3040.1(19) Å ³
Z	2
Density (calculated)	1.333 Mg/m ³
Absorption coefficient	0.456 mm ⁻¹
F(000)	1288
Crystal size	0.300 x 0.020 x 0.010 mm ³
Theta range for data collection	2.920 to 25.094°.
Index ranges	-9<=h<=9, -17<=k<=17, -24<=l<=24
Reflections collected	20938
Independent reflections	8216 [R(int) = 0.0580]
Completeness to theta = 25.094°	98.3 %
Absorption correction	Semi-empirical from equivalents
Refinement method	Full-matrix least-squares on F ²
Data / restraints / parameters	8216 / 524 / 875
Goodness-of-fit on F²	1.049
Final R indices [I>2sigma(I)]	R1 = 0.0661, wR2 = 0.1812
R indices (all data)	R1 = 0.0986, wR2 = 0.2010
Extinction coefficient	n/a
Largest diff. peak and hole	0.901 and -0.673 e.Å ⁻³

Table S19. Crystal data and structure refinement for molecule 7 (inverted wing conformation structure).

Identification code	rcb_t2_cs2_mek
Empirical formula	C40 H30 F0.25 N6 O2 S6 Si
Formula weight	851.90
Temperature	296(2) K
Wavelength	0.77490 Å
Crystal system	Triclinic
Space group	P -1
Unit cell dimensions	a = 9.2847(11) Å α = 80.301(9)°
	b = 14.9183(18) Å β = 78.544(8)°
	c = 22.514(3) Å γ = 87.708(8)°
Volume	3012.5(6) Å ³
Z	4
Density (calculated)	1.878 Mg/m ³
Absorption coefficient	0.554 mm ⁻¹
F(000)	1761
Theta range for data collection	1.51 to 23.88°
Index ranges	-9<=h<=9, -15<=k<=15, -23<=l<=23
Reflections collected	22754
Independent reflections	6873 [R(int) = 0.1003]
Completeness to theta = 23.88°	95.3 %
Refinement method	Full-matrix least-squares on F ²
Data / restraints / parameters	6873 / 96 / 624
Goodness-of-fit on F²	1.775
Final R indices [I>2sigma(I)]	R1 = 0.1890, wR2 = 0.4746
R indices (all data)	R1 = 0.2376, wR2 = 0.4918
Largest diff. peak and hole	0.959 and -0.799 e.Å ⁻³

References

- ¹ Welch, G. C.; Bakus, R. C., II; Teat, S. J.; Bazan, G. C. *J. Am. Chem. Soc.* **2013**, *135*, 2298–2305.
- ² Zhugayevych, A.; Postupna, O.; Bakus, R. C., II; Welch, G. C.; Bazan, G. C.; Tretiak, S. *J. Phys. Chem. C* **2013**, *117*, 4920–4930.
- ³ Sun, Y.; Welch, G. C.; Leong, W. L.; Takacs, C. J.; Bazan, G. C.; Heeger, A. J. *Nature Materials* **2011**, *10*, 1–5.
- ⁴ Takacs, C. J.; Sun, Y.; Welch, G. C.; Perez, L. A.; Liu, X.; Wen, W.; Bazan, G. C.; Heeger, A. J. *J. Am. Chem. Soc.* **2012**, *134*, 16597–16606.